The design of transcription factor-based inhibitors to target Myc: drop the Myc!

Ellenbroek, B.D.

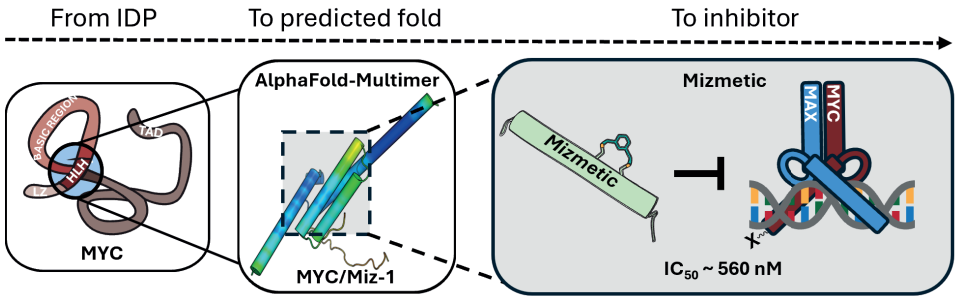

Adapted from: B. D. Ellenbroek, A. S. S. Tirtosentono, S. J. Pomplun, "AlphaFold-Guided Discovery of an Overlapping MYC/Miz-1 Interface Enables Peptidomimetic Disruption of MYC/MAX" *ChemMedChem* **2025**, e202500740.

The data not included in this thesis (e.g. uncut gels) can be found online: https://chemistry-europe.onlinelibrary.wiley.com/doi/10.1002/cmdc.202500740

Chapter 5

AlphaFold-Guided Discovery of an Overlapping MYC/Miz-1 Interface Enables Peptidomimetic Disruption of MYC/MAX

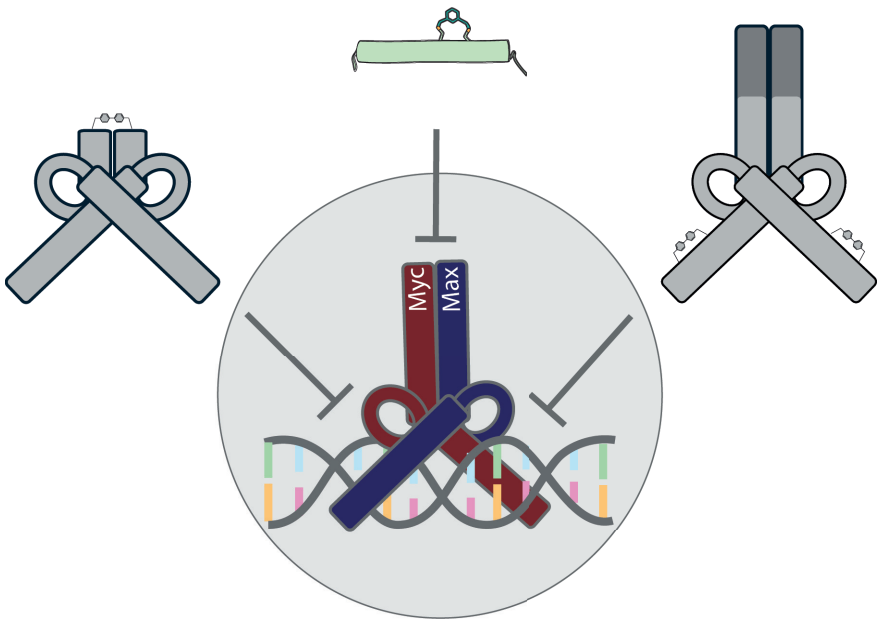

Authors:

Brecht D. Ellenbroek, Amardhiko S.S. Tirtosentono, Sebastian Pomplun

Abstract

Intrinsically disordered proteins (IDPs) lack stable structure and classical binding pockets, making them remarkably difficult to drug. However, upon interacting with partner proteins, IDPs can form transient yet specific and defined interfaces, which, if discovered, can become exploitable footholds for therapeutic intervention. Here, we use AlphaFold-Multimer to shine light on the underexplored oncogenic protein-protein interaction between MYC and Miz-1. Notably, AlphaFold-Multimer predicted that Miz-1 binds at a site overlapping with the MYC/MAX dimerization domain which is MYC's best-characterized oncogenic interface. Guided by this prediction, we designed and synthesized stapled peptidomimetics, targeting the MYC/Miz-1 and MYC/MAX interface. Our best variant, *Mizmetic* 2, binds MYC and alanine scanning identified key binding hotspots and promising sites for beneficial substitutions. The optimized variants disrupted MYC/MAX complex formation and prevented MYC from binding its canonical E-box DNA elements in vitro, with submicromolar potency. MAX/MAX DNA complex formation was also reduced, likely indicating some degree of unspecific binding. While still at a proof-of-concept stage, our findings showcase how AI-based structure prediction can illuminate disordered protein interactions and reveal new targetable sites on MYC.

5.1 Introduction

Protein-protein interactions (PPIs) usually entail large interaction interfaces. While many PPIs are involved in disease, these interactions are difficult to target. [1] The challenge becomes even more critical when intrinsically disordered regions (IDRs) or proteins (IDPs) are involved. IDRs and IDPs can adopt defined conformations when interacting with partner proteins, but their general disordered nature makes structure elucidation approaches very challenging. With approximately 22% of the human genome being an IDP or containing IDRs,[2] it is essential to identify and characterize how these proteins interact in order to target disease related IDPs. Recently more promising in silico strategies were reported, using AlphaFold[3] or RFDiffusion,[4] to predict how IDRs interact with protein partners with a high accuracy[5] or even design de novo interaction partners.[4] Yet, to enable therapeutic development further research is needed.

A well characterized disease related IDP is MYC. Dysregulation of MYC is involved in more than 50% of all human cancers. MYC belongs to the basic-helix-loop-helix leucine zipper (bHLH-LZ) protein family.[6,7] It needs to heterodimerize with protein partners, such as MYC associated protein X (MAX) (**Figure 5.1a**), to bind enhancer-box DNA (E-box, CACGTG) and regulate downstream genes through its disordered transactivation domain (TAD). When not in complex, MYC is disordered (**Figure 5.1a**).

MYC also drives tumor development in complex with MYC interacting Zinc Finger 1 (Miz-1, **Figure 5.1a**).[8,9] It was found that Miz-1 accumulates at MYC target sites.[8] Additionally, overexpression of the mutant MYC^{V394D}, unable to bind to Miz-1 but not impairing MYC/MAX dimerization, in transgenic mice resulted in delayed tumor development.[10,11] This indicated the involvement of the MYC/Miz-1 interaction in cancer. Through two-hybrid studies Peukert *et al.* identified that Miz-1 contains two MYC interacting domains (MID), MID1 and MID2, that interact with MYCs HLH domain (**Figure 5.1a-b**), but not with MAX.[12] Structure predictions suggested that the Miz-1 MID2 domain adopts an amphipathic α-helix that can interact with the HLH domain of MYC.[12]

When MYC binds Miz-1, it becomes a repressor (e.g. of the negative cell cycle regulators $P21^{Cip1}$ and $P15^{ink4b}$) and inhibits cell differentiation. [13–15] The influence of MAX on this interplay is not fully understood yet. Whereas several literature reports found that a ternary complex between MYC/MAX and Miz-1 can be formed, other reports show that Miz-1 and MAX do compete for MYC.[8,12,16,17] In either scenario these data point out the MYC/Miz-1 interface as a promising site for therapeutic targeting.

Despite its critical involvement in cancer MYC is difficult to target with classical drugs. While there are small molecules developed that prevent MYC/MAX formation,[18,19] stabilize MAX/MAX formation,[20] promote MYC degradation[21] or protein-based

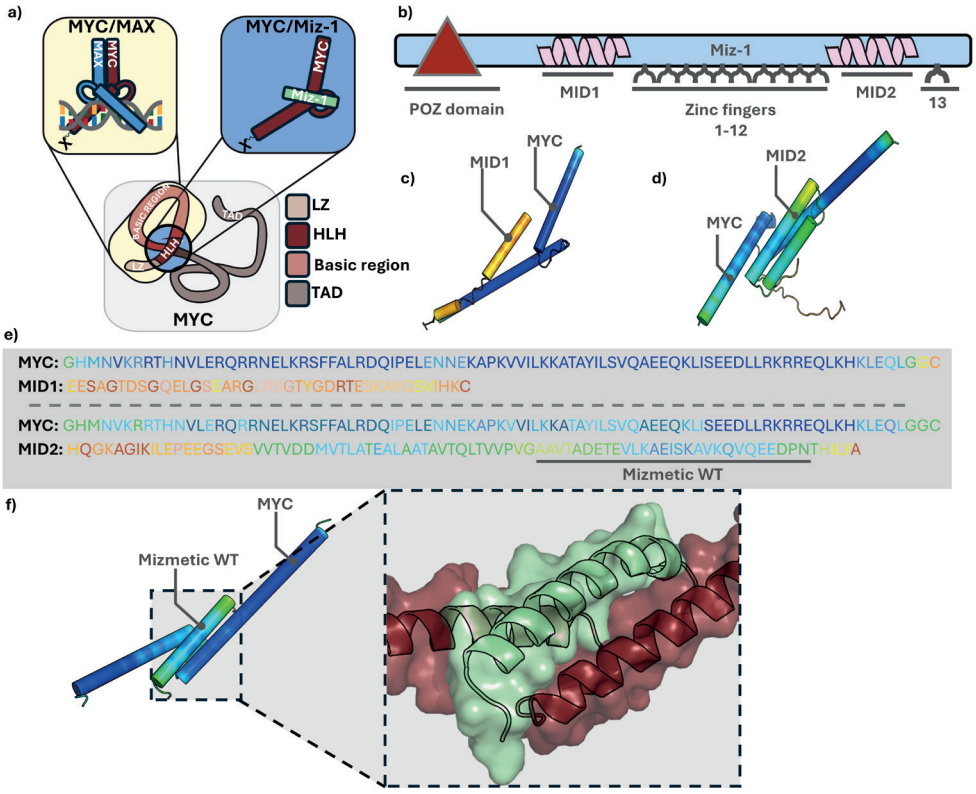

▲Figure 5.1: AlphaFold predicts that a section of 28 residues within MID2 can interact with MYCs HLH domain. a) A schematic representation of MYC and its interaction partners MAX and Miz-1. MAX and Miz-1 have an overlapping interaction site (Blue). MYC contains a transactivation domain (TAD, represented by X), basic region, Helix-Loop-Helix domain (HLH) and a Leucine Zipper (LZ) domain. MYC is disordered when not in complex. When interacting with protein partners it becomes ordered. b) A schematic representation of Miz-1. Miz-1 contains a Poxvirus and Zinc finger (POZ) domain, MYC interacting domain 1 (MID1), 13 zinc fingers and a MID2 domain. c) AlphaFold prediction between MID1 and MYC. ipTM = 0.07, pTM = 0.49. d) AlphaFold prediction between MID2 and MYC. ipTM = 0.33, pTM = 0.47 e) Sequences of MYC, MID1 and MID2 with corresponding coloring scheme for the AlphaFold predictions. Underlined: isolated 28mer, *Mizmetic* WT. f) AlphaFold prediction between *Mizmetic* WT and MYC. ipTM = 0.5 pTM = 0.59. Miz-1 (green) binds with its hydrophobic residues in the HLH domain of MYC (red). AlphaFold per-atom confident score color codes (pLDDT): Dark blue - Very high (pLDDT > 90), Cyano - Confident (90 > pLDDT > 70), Yellow - Low (70 > pLDDT > 50), Orange - Very low (pLDDT < 50). All AlphaFold predictions were performed with $MYC_{369-454}$ and the structures were generated with Pymol.

moieties that inhibit MYC function by blocking the E-box sequence,[7,22–27] no approved drugs are available. Moreover, no modalities targeting the MYC/Miz-1 interaction have been described and there is no crystal structure elucidated for this complex.

Here, we used AlphaFold-Multimer[4] to explore the structural features of the MYC/Miz-1 interaction and its potential druggability. AlphaFold predicted a region of 28amino acids in Miz-1 to bind to the HLH domain of MYC. We synthesized the peptide and demonstrated binding to MYC via biolayer interferometry (BLI). Alanine scanning and rational chemical modifications with helix stabilizing peptide staples guided us to an optimized peptidomimetic (*Mizmetic* 2) and variants able to not only bind to the Miz-1 site but also to disrupt MYC/MAX/DNA binding. Overall, our findings show that AlphaFold-Multimer is a powerful platform to analyze IDRs and their PPIs with potential for identifying novel druggable sites in challenging targets like MYC.

5.2 Results and discussion

5.2.1 AlphaFold predicts MID2 to bind MYC in its HLH domain

The MYC–Miz-1 interaction is difficult to characterize experimentally due to the intrinsically disordered nature of MYC. Peukert *et al.* proposed that Miz-1 engages MYC through an amphipathic α-helix within MYC's HLH domain (**Figure 5.1a**).[15] Bédard *et al.* further showed that the MID2 region of Miz-1 (Miz-$1_{637\text{-}718}$, 84 amino acids) binds more strongly to MYC than MID1 (Miz-$1_{269\text{-}308}$, 42 amino acids).[20] However, the precise structural basis of these interactions remains unknown.

We used AlphaFold-Multimer to model MYC/MID1 (Miz-$1_{269\text{-}308}$, $MYC_{369\text{-}454}$, **Figure 5.1c&e**) and MYC/MID2 complexes (Miz-$1_{637\text{-}718}$, $MYC_{369\text{-}454}$,**Figure 5.1d&e**). AlphaFold did not predict any high-confidence binding mode for MID1 associated to MYC (**Figure 5.1c,** ipTM = 0.07, pTM = 0.49). In contrast, for MID2, AlphaFold predicted, with higher confidence (ipTM = 0.33**,** pTM = 0.47) a 28-residue α-helical segment binding in the hydrophobic groove formed by the MYC HLH domain (**Figure 5.1d**). This predicted binding mode aligns well with the hypothesis proposed by Peukert *et al.*[15] Based on these results, we focused subsequent analyses exclusively on MID2.

We performed a second AlphaFold prediction between MYC and the highest scoring sequence section of MID2 (Miz-$1_{685\text{-}712}$ = *Mizmetic* WT, $MYC_{369\text{-}454}$, ipTM = 0.5 pTM = 0.59, **Figure 5.1f**). This prediction showed a similar fold between *Mizmetic* WT and MYC with the hydrophobic residues of *Mizmetic* WT facing towards a hydrophobic region in the MYC HLH domain.

Experimental binding assays confirmed the MYC/MID2 interaction. To experimentally validate the binding between the two protein domains, we expressed and purified the bHLH-LZ region of MYC (**Figure S5.1-6**, **Table S5.1**, $MYC_{369\text{-}454}$). We synthesized *Mizmetic* WT via solid phase peptide synthesis (SPPS) and biotinylated the N-terminus (**Figure S5.1-6**, **Table S5.1**) for immobilization on the BLI biosensors. BLI indicated

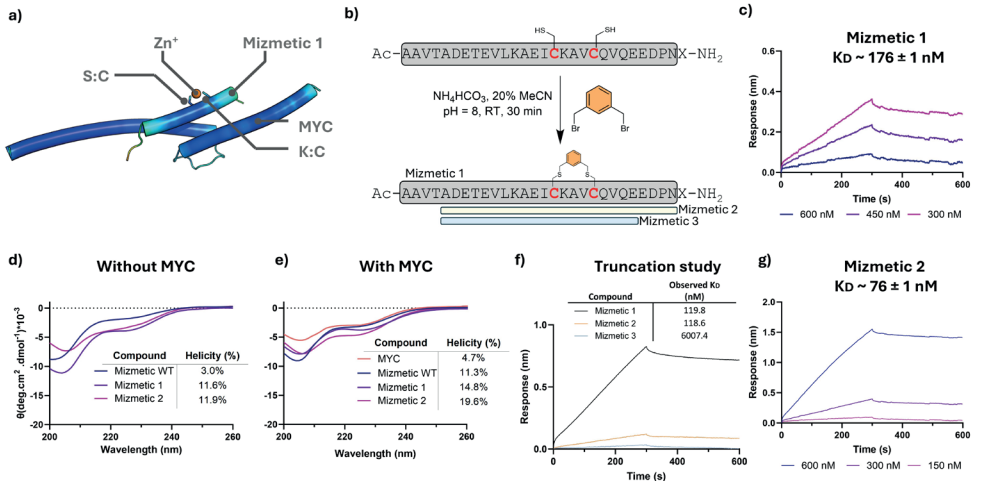

▲Figure 5.2: The incorporation of an i, i+4 staple improves binding of *Mizmetic* to MYC. a) AlphaFold prediction between *Mizmetic* 1 and $MYC_{353–434}$. Serine16 and Lys20 are mutated to a cysteine allowing the incorporation of an artificial staple within AlphaFold. ipTM = 0.67, pTM = 0.68. b) Exemplary stapling reaction. X = β-alanine – Lysin(biotin) linker c) Binding evaluation of *Mizmetic* 1 by BLI. d) Structural characterization of *Mizmetic* WT, 1 and 2 with CD. *Mizmetic* WT shows mainly a random coil, *Mizmetic* 1 and 2 display a CD spectrum of a partial α-helix without MYC. e) Structural characterization of *Mizmetic* WT, 1 and 2 with CD in complex with MYC. A modest increase in α-helicity is observed around 222 nm. Helicities (%) were calculated with BestSEL analysis tool.[42,43] f) Binding evaluation of *Mizmetic* 1, 2 and 3 by BLI. All peptides were screened against 300 nM. *Mizmetic* 3 displayed a 50 times decrease in binding compared to *Mizmetic* 1. g) Binding evaluation of *Mizmetic* 2 with BLI. AlphaFold per-atom confident score color codes: Dark blue - Very high (plDDT > 90), Cyano - Confident (90 > pLDDT > 70), Yellow - Low (70 > pLDDT > 50), Orange - Very low (pLDDT < 50). All AlphaFold predictions were performed with $MYC_{369-454}$ and the structures were generated with Pymol.

that this peptide binds to MYC with an observed affinity of 4.6 µM ± 1.3 µM (**Figure S5.7**, **Table S5.2**), confirming an interaction between the two proteins. However, non-ideal binding behavior was observed by BLI, eventually caused by aggregation of the unstructured MYC domain to the tip when the analyte is bound.[31] We optimized the BLI assay conditions, in order to not observe any unspecific binding of MYC to the unfunctionalized biosensors. However, for the assays with Biotin-*Mizmetic* on the biosensors, further attempts to optimize the binding behavior, including increasing concentrations of blocking reagents or decreasing bound *Mizmetic* analytes, did not improve the shapes of the BLI curves, thereby limiting us in finding the true affinity value towards MYC. Keeping this limitation in mind, in the following text we will refer to observed KDs and in the following experiments we mainly made relative comparisons between the binding affinities rather than referring to absolute values.

5.2.2 Stapling of the Miz-1 helix improves binding to MYC

Both prior studies[15,20] and our AlphaFold predictions suggest that the MID2 region of Miz-1 adopts an α-helical conformation upon binding to MYC. We therefore hypothesized that conformational stabilization through α-helix stapling could enhance the structural rigidity of our *Mizmetic* construct and thereby improve its binding affinity for MYC.[28,32–40] Peptide stapling typically involves covalently linking two residues one or two helical turns apart (i, i + 4 or i, i + 7, respectively), locking the α-helical conformation. To explore optimal stapling positions, we employed AlphaFold modeling. Because AlphaFold does not support non-natural modifications, we mimicked helix stabilization by introducing two cysteines at positions i and i + 4 to coordinate a zinc ion. Cysteine – Zinc coordination is found as a helix stabilizing element in natural proteins, such as Zinc Fingers.[41] Ser16 and Lys20 were chosen as mutation sites, as these residues are located on the solvent-exposed "back" of the helix and are not predicted to participate in MYC binding (**Figure 5.2a**).

The AlphaFold prediction for the zinc-coordinated mutant showed an even higher confidence score compared to the unstapled construct (ipTM = 0.5, pTM = 0.59 vs. ipTM = 0.67, pTM = 0.68, **Figure 5.2a**). Based on these results, we synthesized *Mizmetic 1* with Ser16 and Lys20 replaced by cysteines, followed by thiol–aromatic crosslinking using *m*-bromoxylene to generate a covalent i, i + 4 staple (**Figure S5.1-10**, **Table S5.1**).[44,45] The reaction scheme and final product, *Mizmetic* 1, are shown in**Figure 5.2b**.

BLI indicated an increase in binding affinity for *Mizmetic* 1 compared to *Mizmetic* WT (**Figure 5.2c**). A full concentration curve displayed an observed K_D of ~ 176 ± 1 nM by BLI. When compared to *Mizmetic* WT (observed K_D ~ 4.6 μM ± 1.3 μM), this is a 26x improvement in binding, upon incorporation of the staple (**Table S5.2**).

Circular Dichroism (CD) spectroscopy was used to asses α-helicity (**Figure 5.2d-e**). Mizmetic WT displayed mainly a pattern that is characteristic for a random coil in the absence of MYC (**Figure 5.2d**, **Figure S5.8**), whereas Mizmetic 1 showed partial α-helicity with minima at 208 nm and 222 nm. BestSEL analysis[37,38] estimated helicity at 3.0% for Mizmetic WT and 11.6% for Mizmetic 1 (**Figure 5.2d**, **Figure S5.8**). MYC alone displayed 4.7% helicity (**Figure 5.2e**, **Figure S5.8**). Upon complex formation, both Mizmetic*s* showed increased helical content (**Figure 5.2e**, **Figure S5.8**).

To further optimize Mizmetic 1 we sought to determine the minimal sequence necessary for binding. Therefore, a stepwise truncation study was performed. This showcased that four amino acids at the N-terminus could be removed (Mizmetic 2, observed K_D ~ 118.6 nM, **Figure 5.2f**, **Table S5.3**) whereas an additional deletion of four amino acids at the C-terminus resulted in a drop in observed affinity according to BLI (Mizmetic 3, observed K_D ~ 6007.4 nM,

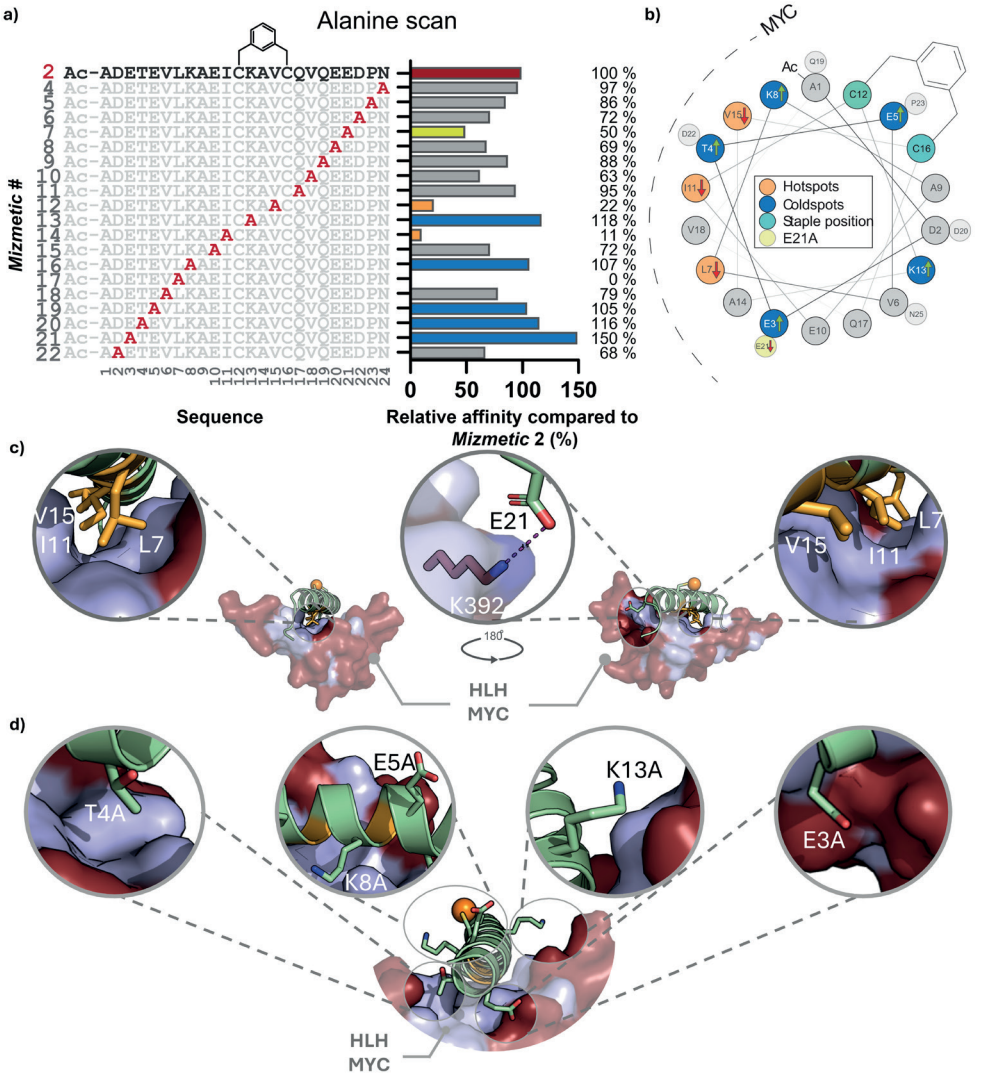

▲Figure 5.3: T The alanine scan highlighted three hotspot and five coldspot positions that are important for *Mizmetic*/MYC interaction. a) All stapled *Mizmetic* 2 alanine analogues were screened against 400 nM MYC. The alanine mutation is highlighted in red. The relative increase/decrease in affinity compared to the Kᴅ of *Mizmetic* 2 are displayed. b) The α-helical wheel of *Mizmetic* 2 shows that the hotspots are facing the same side of the *Mizmetic* peptide and are flanked by E3, T4 and K8. c) On the left and right three hotspots are enlarged (orange) and are interacting in a hydrophobic region within the HLH domain. In the middle a potential ionic interaction between Mizmetic^{E21} and MYC^{K392} is enlarged. d) Amplification of the coldspot residues with an affinity of >100% compared to *Mizmetic* 2. In red is the HLH domain of MYC depicted. In light blue the hydrophobic residues within the HLH domain. The HLH domain of MYC is portrayed in red with hydrophobic residues highlighted in light blue. All experiments with expressed $MYC_{369-454}$ and the structures were generated with Pymol.

Figure 5.2f, **Table S5.3**). A full concentration curve displayed an observed affinity of ~76 ± 1 nM for the stapled 24mer Mizmetic 2 according to BLI (**Figure 5.2g**).

Similar to Mizmetic 1, CD spectra indicated that Mizmetic 2 adopts a partially folded α-helix in the absence of MYC (**Figure 5.2d**, **Figure S5.8**). Notably, almost 20% of helicity was observed when incubated with MYC (**Figure 5.2e**, **Figure S5.8**). The formation of a partial α-helix combined with the increase in affinity indicate that the staple might promote the correct orientation of the interacting residues of Mizmetic 1 and 2 to bind MYC but is unable to promote a full α-helix as is observed when MYC and MAX are incubated together.[7,27]

5.2.3 Alanine scanning showcased three hotspots and five coldspots

We next wanted to assess the influence of each individual amino acid of Mizmetic 2 by means of an alanine scan. We synthesized 19 alanine mutants (Mizmetic 4-22) and measured BLI at a single concentration to compare their relative affinity to Mizmetic 2 (**Figure 5.3a, Figure S5.9**, **Table S5.4**). For most positions the alanine substitution did not influence binding considerably. Alanine mutants for Leu7, Ile11 and Val15 significantly weakened binding, indicating the importance of these positions for binding to MYC. The helical wheel shows that these residues are facing the same side (**Figure 5.3b**). This observation supports the predicted AlphaFold simulation as these three hydrophobic residues were predicted to interact deeply within the hydrophobic surface of the HLH domain of MYC (**Figure 5.3c**, **orange**). Additionally, a 2-fold decrease in affinity was observed for E12A (**Figure 5.3a**). In the AlphaFold predictions this residue was facing towards MYC (**Figure 5.3c**, **middle**), potentially forming a salt bridge with K392.

Five alanine mutants displayed slightly increased binding: Glu3, Thr4, Glu5, Lys8 and Lys13. The α-helical wheel of Mizmetic 2 shows that the hydrophobic surface is flanked by Glu3, Thr4 and Lys8 (**Figure 5.3b**). Whereas Glu3 and Lys13 are predicted to face away from MYC, Thr4 and Lys8 are predicted to face towards a hydrophobic region (**Figure 5.3d**). This could explain the increase in affinity for T4A and K8A as these positions become more apolar when mutated to an alanine. E5A and K8A could potentially form an intramolecular salt-bridge that is unfavorable for Mizmetic/MYC binding (**Figure 5.3d**), resulting in alanine mutants with increased affinity. Overall, our alanine scan indicated hotspot residues, in good agreement with the AlphaFold prediction and in addition, unexpectedly it resulted in the identification of a few variants with increased affinity.

5.2.4 Mizmetic alanine analogues can inhibit MYC-MAX-DNA binding

While our Mizmetic compounds bind to the Miz-1 binding site on MYC, we set out to explore if these compounds facilitate the inhibition of the most prominent

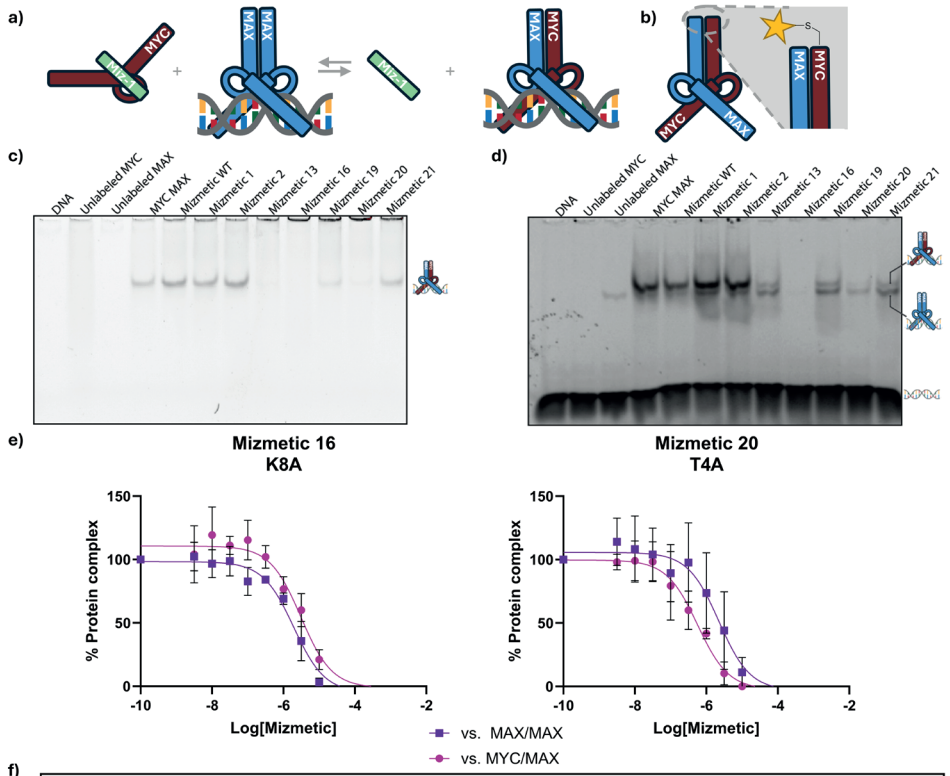

f)

#	Sequence	IC_{50} MYC MAX (μM)	IC_{50} MAX MAX (μM)	Ratio
16	Ac-ADETEVL**A**AEICKAVCQVQEEDPN - X	3.08±1.94	1.94±0.71	0.6
20	Ac-ADE**A**EVLKAEICKAVCQVQEEDPN - X	0.56 ±0.22	2.25±1.93	4

▲Figure 5.4: Mizmetic alanine analogues can inhibit MYC/MAX and MAX/MAX complex formation. a) It is suggested that Miz-1 and Max compete to bind MYC. We hypothesized that Mizmetics can inhibit MYC/MAX complex formation. b) MYC and MAX can be labeled with Fluorescein-5-maleimide without interfering with complex formation. c) EMSA essay with labeled MYC (DNA construct: TTC CT**C ACG TG**G CAT TTG GGT GC**C ACG TG**A GG). MYC/MAX binding can be inhibited by Mizmetic 13, 16 and 20. d) EMSA assay with labeled DNA (DNA construct: IRD700-ACC CCA C**CA CGT G**GT GCC T). The MYC/MAX/DNA complex can be inhibited by Mizmetic 13, 16, 20 and 21. Mizmetic 13 and 20 show partial selectivity, whereas Mizmetic 16 shows complete inhibition. e&f) Concentration curves with Mizmetics 16 and 20. Competition assay was performed in independent triplicates. EMSA displays for Mizmetic 16 (K8A) no selectivity between MYC/MAX or MAX/MAX. Mizmetic 20 (T4A) displays moderate specificity for MYC over MAX. X = β-alanine + Lysine(biotin) linker.

cancer driving PPI: the MYC/MAX interaction. It has been proposed that a ternary complex forms in which MYC binds both Miz-1 and MAX.[8,12,16] Contrarily, it has also been proposed that Miz-1 and MAX compete for MYC interaction (**Figure 5.4a**).[17] Our AlphaFold simulations support the latter hypothesis, and therefore we hypothesized that our Mizmetic compounds could inhibit

the MYC/MAX dimer formation and with that their binding to E-Box DNA.

We used native electrophoretic mobility shift assay (EMSA) to study the potential inhibition of the protein-protein-DNA complex. We labeled MYC (MYC_F, **Figure S5.1-5.6**) with Fluorescein-5-maleimide at its C-terminal cysteine (**Figure 5.4b**). EMSA did confirm MYC/MAX/DNA formation (**Figure 5.4c** lane MYC/MAX and **Figure S5.10**). Subsequently, we incubated MYC_F and Max with either Mizmetic WT, 1, 2 as well as with the improved alanine analogues (Mizmetic 13, 16, 19-21, **Figure 5.4c**). While EMSA showed that Mizmetic WT, 1 and 2 did not inhibit MYC/MAX complex formation, variants 13, 16, and 20 resulted in complete disappearance of the MYC/MAX/DNA band, and also variants 19 and 21 show slight inhibition

In order to observe both MYC/MAX and MAX/MAX DNA complexes at the same time, we performed EMSAs also with unlabeled proteins and IRD700-labeled E-Box DNA. While of similar size, MAX/MAX/DNA and MYC/MAX/DNA caused bands at distinguished heights on the gel. With the hypothesis of Mizmetics binding to MYC[12,17] we expected to still see the MAX/MAX band (slightly below MYC/MAX) upon MYC/MAX inhibition. In accordance with the previous experiment we did not observe MYC/MAX/DNA inhibition for Mizmetic WT, 1 and 2. (**Figure 5.4d**), All alanine analogues, as seen before, displayed inhibition. For variants 13, 19, 20 and 21 the MYC/MAX/DNA band was substantially reduced (or even absent in 20), while a clear MAX/MAX/DNA band was visible. For Mizmetic 16 no protein/DNA complex was observed at all, potentially indicating some degree of unspecific binding.

To further investigate the specificity of the selected variants, we measured full DNA binding curves with inhibitor added to either MYC/MAX or MAX/MAX. For the visualization and quantification of the bands in the EMSA gels we used either labeled MYC (for MYC/MAX) or labeled MAX (MAX_F, **Figure S5.1-5.6**, for MAX/MAX) (**Figure 5.4e-f**, **Figures S5.11-5.13**). In accordance with the single point EMSA, Mizmetic 16 had no preference for MYC over MAX, displaying IC_{50}s of ~3 µM and ~2 µM, respectively. Mizmetic 20 inhibited MYC/MAX with an IC_{50} of 560 nM, 4-fold more potent than it's inhibitory activity measured for the MAX/MAX complex (**Figure 5.4e-f**).

After the observation that Mizmetic 16 and 20 also inhibited MAX/MAX/DNA we tested direct binding to MAX with BLI (**Figure S5.14**). However, no direct binding to MAX was observed at a similar concentration as MYC. MAX hypothetically exists as a dimer in solution and thus would block the binding site of both Mizmetics thereby preventing binding. Based on these data, we cannot fully explain what causes the unspecific binding in the EMSA competition assays.

5.3 Conclusion

Intrinsically disordered proteins (IDPs) remain one of the most elusive classes of

drug targets, yet their disorder often conceals well-defined structures that emerge upon binding in protein-protein complexes. Using AlphaFold-Multimer, we characterized the MYC/Miz-1 interaction, revealing a defined α-helical interface within Miz-1 MID2 that overlaps with the canonical MYC/MAX dimerization site. Guided by this model, we designed and optimized stapled Miz-1–derived peptidomimetics,improving binding affinity from micromolar to low-nanomolar potency. Alanine scanning validated AlphaFold's predicted hotspots and revealed substitutions that further enhanced activity. Notably, select variants disrupted MYC/MAX/DNA binding with submicromolar potency, highlighting a novel mode of intervention against a transcription factor long considered "undruggable." While our work remains at a proof-of-concept stage, it establishes a strategy for targeting transient but structurally precise IDP interfaces, offering a promising foothold for future therapeutic development against MYC-driven cancers.

5.4 References

[1] J. Oláh, T. Szénási, A. Lehotzky, V. Norris, J. Ovádi, "Challenges in Discovering Drugs That Target the Protein-Protein Interactions of Disordered Proteins." *Int J Mol Sci* **2022**, *23*, 1550.

[2] K. Kosoglu, Z. Aydin, N. Tuncbag, A. Gursoy, O. Keskin, "Structural coverage of the human interactome." *Brief Bioinform* **2023**, *25*, 1–11.

[3] C. Agoni, R. Fernández-Díaz, P. B. Timmons, A. Adelfio, H. Gómez, D. C. Shields, "Molecular Modelling in Bioactive Peptide Discovery and Characterisation." *Biomolecules* **2025**, *15*, 524.

[4] J. Jumper, R. Evans, A. Pritzel, T. Green, M. Figurnov, O. Ronneberger, K. Tunyasuvunakool, R. Bates, A. Žídek, A. Potapenko, A. Bridgland, C. Meyer, S. A. A. Kohl, A. J. Ballard, A. Cowie, B. Romera-Paredes, S. Nikolov, R. Jain, J. Adler, T. Back, S. Petersen, D. Reiman, E. Clancy, M. Zielinski, M. Steinegger, M. Pacholska, T. Berghammer, S. Bodenstein, D. Silver, O. Vinyals, A. W. Senior, K. Kavukcuoglu, P. Kohli, D. Hassabis, "Highly accurate protein structure prediction with AlphaFold." *Nature* **2021**, *596*, 583–589.

[5] K. Wu, H. Jiang, D. R. Hicks, C. Liu, E. Muratspahić, T. A. Ramelot, Y. Liu, K. McNally, S. Kenny, A. Mihut, A. Gaur, B. Coventry, W. Chen, A. K. Bera, A. Kang, S. Gerben, M. Y.-L. Lamb, A. Murray, X. Li, M. A. Kennedy, W. Yang, Z. Song, G. Schober, S. M. Brierley, J. O'Neill, M. H. Gelb, G. T. Montelione, E. Derivery, D. Baker, "Design of intrinsically disordered region binding proteins" *Science (1979)* **2025**, *389*, eadr8063.

[6] H. Bret, J. Gao, D. J. Zea, J. Andreani, R. Guerois, "From interaction networks to interfaces, scanning intrinsically disordered regions using AlphaFold2." *Nat Commun* **2024**, *15*, 597.

[7] A. Omidi, M. H. Møller, N. Malhis, J. M. Bui, J. Gsponer, "AlphaFold-Multimer accurately captures interactions and dynamics of intrinsically disordered protein regions." *Proc Natl Acad Sci U S A* **2024**, *121*, e2406407121.

[8] D. Piovesan, A. M. Monzon, S. C. E. Tosatto, "Intrinsic protein disorder and conditional folding in AlphaFoldDB." *Protein Sci* **2022**, *31*, e4466.

[9] S. K. Nair, S. K. Burley, "X-ray structures of Myc-Max and Mad-Max recognizing DNA. Molecular bases of regulation by proto-oncogenic transcription factors." *Cell* **2003**, *112*, 193–205.

[10] S. Pomplun, M. Jbara, C. K. Schissel, S. Wilson Hawken, A. Boija, C. Li, I. Klein, B. L. Pentelute, "Parallel Automated Flow Synthesis of Covalent Protein Complexes That Can Inhibit MYC-Driven Transcription." *ACS Cent Sci* **2021**, *7*, 1408–1418.

[11] S. Peter, J. Bultinck, K. Myant, L. A. Jaenicke, S. Walz, J. Müller, M. Gmachl, M. Treu, G. Boehmelt, C. P. Ade, W. Schmitz, A. Wiegering, C. Otto, N. Popov, O. Sansom, N. Kraut, M. Eilers, "Tumor cell-specific inhibition of MYC function using small molecule inhibitors of the HUWE1 ubiquitin ligase." *EMBO Mol Med* **2014**, *6*, 1525–1541.

[12] K. E. Wiese, S. Walz, B. von Eyss, E. Wolf, D. Athineos, O. Sansom, M. Eilers, "The role of MIZ-1 in MYC-dependent tumorigenesis." *Cold Spring Harb Perspect Med* **2013**, *3*, a014290.

[13] J. Van Riggelen, J. Müller, T. Otto, V. Beuger, A. Yetil, P. S. Choi, C. Kosan, T. Möröy, D. W. Felsher, M. Eilers, "The interaction between Myc and Miz1 is required to antagonize TGFβ-dependent autocrine signaling during lymphoma formation and maintenance" *Genes Dev* **2010**, *24*, 1281.

[14] S. Herold, M. Wanzel, V. Beuger, C. Frohme, D. Beul, T. Hillukkala, J. Syvaoja, H.-P. Saluz, F. Haenel, M. Eilers, "Negative regulation of the mammalian UV response by Myc through association with Miz-1." *Mol Cell* **2002**, *10*, 509–521.

[15] K. Peukert, P. Staller, A. Schneider, G. Carmichael, F. Hänel, M. Eilers, "An alternative pathway for gene regulation by Myc." *EMBO J* **1997**, *16*, 5672–5686.

[16] P. Staller, K. Peukert, A. Kiermaier, J. Seoane, J. Lukas, H. Karsunky, T. Möröy, J. Bartek, J. Massagué, F. Hänel, M. Eilers, "Repression of p15INK4b expression by

Myc through association with Miz-1." *Nat Cell Biol* **2001**, *3*, 392–399.

[17] J. Seoane, C. Pouponnot, P. Staller, M. Schader, M. Eilers, J. Massagué, "TGFβ influences Myc, Miz-1 and Smad to control the CDK inhibitor p15INK4b" *Nat Cell Biol* **2001**, *3*, 400–408.

[18] G. F. Claassen, S. R. Hann, "A role for transcriptional repression of p21CIP1 by c-Myc in overcoming transforming growth factor beta -induced cell-cycle arrest." *Proc Natl Acad Sci U S A* **2000**, *97*, 9498–503.

[19] S. Walz, F. Lorenzin, J. Morton, K. E. Wiese, B. von Eyss, S. Herold, L. Rycak, H. Dumay-Odelot, S. Karim, M. Bartkuhn, F. Roels, T. Wüstefeld, M. Fischer, M. Teichmann, L. Zender, C.-L. Wei, O. Sansom, E. Wolf, M. Eilers, "Activation and repression by oncogenic MYC shape tumour-specific gene expression profiles." *Nature* **2014**, *511*, 483–7.

[20] M. Bédard, L. Maltais, M. Montagne, P. Lavigne, "Miz-1 and Max compete to engage c-Myc: implication for the mechanism of inhibition of c-Myc transcriptional activity by Miz-1." *Proteins* **2017**, *85*, 199–206.

[21] L. Boike, A. G. Cioffi, F. C. Majewski, J. Co, N. J. Henning, M. D. Jones, G. Liu, J. M. McKenna, J. A. Tallarico, M. Schirle, D. K. Nomura, "Discovery of a Functional Covalent Ligand Targeting an Intrinsically Disordered Cysteine within MYC" *Cell Chem Biol* **2021**, *28*, 4-13.e17.

[22] H. Han, A. D. Jain, M. I. Truica, J. Izquierdo-Ferrer, J. F. Anker, B. Lysy, V. Sagar, Y. Luan, Z. R. Chalmers, K. Unno, H. Mok, R. Vatapalli, Y. A. Yoo, Y. Rodriguez, I. Kandela, J. B. Parker, D. Chakravarti, R. K. Mishra, G. E. Schiltz, S. A. Abdulkadir, "Small-Molecule MYC Inhibitors Suppress Tumor Growth and Enhance Immunotherapy." *Cancer Cell* **2019**, *36*, 483-497.e15.

[23] N. B. Struntz, A. Chen, A. Deutzmann, R. M. Wilson, E. Stefan, H. L. Evans, M. A. Ramirez, T. Liang, F. Caballero, M. H. E. Wildschut, D. V Neel, D. B. Freeman, M. S. Pop, M. McConkey, S. Muller, B. H. Curtin, H. Tseng, K. R. Frombach, V. L. Butty, S. S. Levine, C. Feau, S. Elmiligy, J. A. Hong, T. A. Lewis, A. Vetere, P. A. Clemons, S. E. Malstrom, B. L. Ebert, C. Y. Lin, D. W. Felsher, A. N. Koehler, "Stabilization of the Max Homodimer with a Small Molecule Attenuates Myc-Driven Transcription." *Cell Chem Biol* **2019**, *26*, 711-723.e14.

[24] S. R. Boyd, S. Chamakuri, A. J. Trostle, H. Chen, Z. Liu, A. Jian, J. Wang, A. Malovannaya, D. W. Young, "MYC-Targeting PROTACs Lead to Bimodal Degradation and N-Terminal Truncation." *ACS Chem Biol* **2025**, *20*, 896–906.

[25] L. Soucek, M. Helmer-Citterich, A. Sacco, R. Jucker, G. Cesareni, S. Nasi, "Design and properties of a Myc derivative that efficiently homodimerizes" *Oncogene 1998 17:19* **1998**, *17*, 2463–2472.

[26] B. D. Ellenbroek, J. P. Kahler, D. Arella, C. Lin, W. Jespers, E. A.-K. Züger, M. Drukker, S. J. Pomplun, "Development of DuoMYC: a synthetic cell penetrant miniprotein that efficiently inhibits the oncogenic transcription factor MYC." *Angew Chem Int Ed Engl* **2025**, *64*, e202416082.

[27] I. Inamoto, I. Sheoran, S. C. Popa, M. Hussain, J. A. Shin, "Combining Rational Design and Continuous Evolution on Minimalist Proteins That Target the E-box DNA Site." *ACS Chem Biol* **2021**, *16*, 35–44.

[28] T. E. Speltz, Z. Qiao, C. S. Swenson, X. Shangguan, J. S. Coukos, C. W. Lee, D. M. Thomas, J. Santana, S. W. Fanning, G. L. Greene, R. E. Moellering, "Targeting MYC with modular synthetic transcriptional repressors derived from bHLH DNA-binding domains." *Nat Biotechnol* **2023**, *41*, 541–551.

[29] Z. Z. Brown, C. Mapelli, I. Farasat, A. V Shoultz, S. A. Johnson, F. Orvieto, A. Santoprete, E. Bianchi, A. B. McCracken, K. Chen, X. Zhu, M. J. Demma, B. M. Lacey, K. A. Canada, R. M. Garbaccio, J. O'Neil, A. Walji, "Multiple Synthetic Routes to the Mini-Protein Omomyc and Coiled-Coil Domain Truncations." *J Org Chem* **2020**, *85*, 1466–1475.

[30] M. Jbara, S. Pomplun, C. K. Schissel, S. W. Hawken, A. Boija, I. Klein, J. Rodriguez, S. L. Buchwald, B. L. Pentelute,

"Engineering Bioactive Dimeric Transcription Factor Analogs via Palladium Rebound Reagents." *J Am Chem Soc* **2021**, *143*, 11788–11798.

[31] N. Sherer, J.-H. Cho, "Overcoming Effects of Heterogeneous Binding on BLI Analysis." *ACS Omega* **2025**, *10*, 28422–28428.

[32] C. E. Schafmeister, J. Po, G. L. Verdine, "An All-Hydrocarbon Cross-Linking System for Enhancing the Helicity and Metabolic Stability of Peptides" *J Am Chem Soc* **2000**, *122*, 5891–5892.

[33] A. Kuepper, N. M. McLoughlin, S. Neubacher, A. Yeste-Vázquez, E. Collado Camps, C. Nithin, S. Mukherjee, L. Bethge, J. M. Bujnicki, R. Brock, S. Heinrichs, T. N. Grossmann, "Constrained peptides mimic a viral suppressor of RNA silencing." *Nucleic Acids Res* **2021**, *49*, 12622–12633.

[34] T. Anananuchatkul, I. V. Chang, T. Miki, H. Tsutsumi, H. Mihara, "Construction of a Stapled α-Helix Peptide Library Displayed on Phage for the Screening of Galectin-3-Binding Peptide Ligands." *ACS Omega* **2020**, *5*, 5666–5674.

[35] P. Timmerman, J. Beld, W. C. Puijk, R. H. Meloen, "Rapid and quantitative cyclization of multiple peptide loops onto synthetic scaffolds for structural mimicry of protein surfaces." *Chembiochem* **2005**, *6*, 821–824.

[36] S. Mitra, J. E. Montgomery, M. J. Kolar, G. Li, K. J. Jeong, B. Peng, G. L. Verdine, G. B. Mills, R. E. Moellering, "Stapled peptide inhibitors of RAB25 target context-specific phenotypes in cancer." *Nat Commun* **2017**, *8*, 660.

[37] Z. Qiao, L. C. Nguyen, D. Yang, C. Dann, D. M. Thomas, M. Henn, A. Valdespino, C. S. Swenson, S. A. Oakes, M. R. Rosner, R. E. Moellering, "Direct inhibition of tumor hypoxia response with synthetic transcriptional repressors." *Nat Chem Biol* **2025**, *21*, 247–255.

[38] Q. Chu, R. E. Moellering, G. J. Hilinski, Y.-W. Kim, T. N. Grossmann, J. T.-H. Yeh, G. L. Verdine, "Towards understanding cell penetration by stapled peptides" *Medchemcomm* **2015**, *6*, 111–119.

[39] R. Mourtada, H. D. Herce, D. J. Yin, J. A. Moroco, T. E. Wales, J. R. Engen, L. D. Walensky, "Design of stapled antimicrobial peptides that are stable, nontoxic and kill antibiotic-resistant bacteria in mice." *Nat Biotechnol* **2019**, *37*, 1186–1197.

[40] A. M. Spokoyny, Y. Zou, J. J. Ling, H. Yu, Y.-S. Lin, B. L. Pentelute, "A perfluoroaryl-cysteine S(N)Ar chemistry approach to unprotected peptide stapling." *J Am Chem Soc* **2013**, *135*, 5946–5949.

[41] K. Kluska, J. Adamczyk, A. Krężel, "Metal binding properties of zinc fingers with a naturally altered metal binding site." *Metallomics* **2018**, *10*, 248–263.

[42] A. Micsonai, F. Wien, N. Murvai, M. P. Nyiri, B. Balatoni, Y.-H. Lee, T. Molnár, Y. Goto, F. Jamme, J. Kardos, "BeStSel: analysis site for protein CD spectra—2025 update" *Nucleic Acids Res* **2025**, *53*, W73–W83.

[43] A. Micsonai, É. Moussong, F. Wien, E. Boros, H. Vadászi, N. Murvai, Y.-H. Lee, T. Molnár, M. Réfrégiers, Y. Goto, Á. Tantos, J. Kardos, "BeStSel: webserver for secondary structure and fold prediction for protein CD spectroscopy." *Nucleic Acids Res* **2022**, *50*, W90–W98.

[44] H. Jo, N. Meinhardt, Y. Wu, S. Kulkarni, X. Hu, K. E. Low, P. L. Davies, W. F. DeGrado, D. C. Greenbaum, "Development of α-helical calpain probes by mimicking a natural protein-protein interaction." *J Am Chem Soc* **2012**, *134*, 17704–17713.

[45] P. Timmerman, W. C. Puijk, R. H. Meloen, "Functional reconstruction and synthetic mimicry of a conformational epitope using CLIPS technology." *J Mol Recognit* **2007**, *20*, 283–299.

5.5 Experimental

H_2O used in the experiments was Mili-Q water obtained from Milli-Q® Reference bought at Avantor and will from this point on be mentioned as H_2O.

5.5.1 Synthesis procedures

5.5.1.1 Automated Solid phase peptide synthesis (SPPS) – general protocol

Peptides were prepared using a Syro I XP synthesizer on a Chemmatrix rink amide resin at a 41 µmol, 20 µmol or 10 µmol scale. The same equivalents were utilized for all scales. Resin was always swollen in 1000 µL DMF for 10 min at 70 °C prior to the synthesis.

General 41 µmol SPPS protocol: Amino acids were dissolved to a concentration of 0.4 M in DMF and HATU to 0.36 M in DMF. For each coupling, amino acid solution (7.8 eq., 800 µL), HATU solution (7.0 eq., 800 µL for) and pure DIPEA (28.0 eq., 200 µL) were added to the resin (100 mg, loading capacity of 0.41 mmol/g). Coupling reactions were performed at 70 °C for 8 minutes, followed by washes with DMF (3x 1500 µL). Fmoc removal was performed with 20%:1%:79% = piperidine:Formic acid:DMF (1500 µL, 4 minutes, 70 °C) followed by washes with DMF (3x 1500 µL).

Fmoc-β-Alanine-OH coupling 41 µmol: For Fmoc-β-Alanine-OH coupling different conditions were performed. Fmoc-β-Alanine-OH was dissolved to a concentration of 0.25 M in DMF and HATU to 0.36 M in DMF. For each coupling, amino acid solution (4.9 eq., 800 µL), HATU solution (3.5 eq., 400 µL), pure DIPEA (14 eq., 100 µL) and DMF (500 µL) were added to the resin (100 mg, loading capacity of 0.41 mmol/g). Coupling reactions were performed at 70 °C for 15 minutes, followed by washes with DMF (3x 2000 µL). Fmoc removal was performed with 20%:1%:79% = piperidine:Formic acid:DMF (1800 µL, 7 minutes, 70 °C) followed by washes with DMF (3x 2000 µL).

General 20 µmol SPPS protocol (for 10 µmol 0.5x): Amino acids were dissolved to a concentration of 0.4 M in DMF and HATU to 0.36 M in DMF. For each coupling, amino acid solution (7.8 eq., 400 µL), HATU solution (7.0 eq., 400 µL), pure DIPEA (28.0 eq., 100 µL) and DMF (100 µL) were added to the resin (50 mg, loading capacity of 0.41 mmol/g). Coupling reactions were performed at 70 °C for 8 minutes, followed by washes with DMF (3x 1000 µL). Fmoc removal was performed with 20%:1%:79% = piperidine:Formic acid:DMF (1 mL, 4 minutes, 70 °C) followed by washes with DMF (3x 1000 µL).

Fmoc-β-Alanine-OH coupling 20 µmol scale (for 10 µmol 0.5x): For Fmoc-β-Alanine-OH coupling different conditions were performed. Fmoc-β-Alanine-OH

was dissolved to a concentration of 0.25 M in DMF and HATU to 0.36 M in DMF. For each coupling, amino acid solution (4.8 eq., 400 µL), HATU solution (3.5 eq., 200 µL), pure DIPEA (14.0 eq., 50 µL) and DMF (500 µL) were added to the resin (50 mg, loading capacity of 0.41 mmol/g). Coupling reactions were performed at 70 °C for 30 minutes, followed by washes with DMF (3x 2000 µL). Fmoc removal was performed with 20%:1%:79% = piperidine:Formic acid:DMF (1000 µL, 7 minutes, 70 °C) followed by washes with DMF (3x 2000 µL).

The final crude peptidyl resin was manually washed 3x with DMF followed by 3x DCM, dried by vacuum and either directly cleaved or stored at -20 °C.

5.5.1.2 Fmoc-Lys(biotin)-OH coupling protocol – general protocol

Fmoc-Lys(biotin) was coupled manually either as first building block for C-terminal incorporation or as last building block for N-terminal incorporation. Fmoc-Lys(biotin)-OH coupling was performed on a 10 µmol scale. Fmoc-Lys(Biotin)-OH (21.2 mg, 35.6 µmol, 3.5 eq.) and DIPEA (21.5 µL, 123.2 µmol, 12.3 eq.) were pre-incubated in 1000 µL DMF. To the mixture 1000 µL HATU solution in DMF (12.3 mg, 32.3 µmol, 2.9 eq.) was added and incubated for 1 min. Then, the full preactivated mixture was added to the peptidyl resin (10 µmol, 1eq.) and incubated at room temperature (RT) for 1 hour while shaking at 750 rpm. The resin was drained and washed with DMF (3x 1000 µL). Then, Fmoc removal cocktail 20%:1%:79% = piperidine:Formic acid:DMF, 1.5 mL) was added to the peptidyl resin and incubated at RT for 20 minutes while shaking at 750 rpm. The peptidyl resin was washed 3x with 1000 DMF.

5.5.1.3 Acetylation – general protocol

Dry peptidyl resin was swollen in DMF for 10 minutes prior to the addition of acetylation cocktail (10%:10%:80% = Ac_2O:DIPEA:DMF, 1.5 mL). The peptidyl resin was incubated in cocktail while shaking for 15 minutes at RT, drained under vacuum, washed with DMF (3x mL) and DCM (3x mL) and subsequently dried under vacuum. If not cleaved directly, peptidyl resin was stored at -20 °C.

5.5.1.4 Full cleavage – general protocol

Dry peptidyl resin was cleaved for 2 hours with 2 mL of the following cleavage cocktail: 92.5%:5%:2.5% = TFA:H_2O:TIPS. Then, cleavage cocktail was evaporated under a gentle nitrogen stream (to < 0.5 mL). To the peptide ice cold diethyl ether (~5 mL) was added and peptide was obtained by centrifugation for 5 minutes at 10.000 rpm. Crude peptide pellet was dissolved in 10%:0.1%:89.9% = MeCN:TFA:H_2O and lyophilized.

5.5.1.5 Purification – general protocol

All Mizmetic compounds were purified on a Biotage® Selekt Flash Purification System equipped with a Biotage® Sfär C18 D - Duo 25 g column using UV detection at 214 nm. The following gradient was used: 15% solvent B over 2 column volumes (CV), 15% to 55% solvent B over 10 CV, 55% to 98% solvent B over 0 CV, 98% solvent B over 4 CV with H_2O with 0.1% TFA as Solvent A and MeCN with 0.1%TFA as Solvent B. Fractions were analyzed by LC-MS.

5.5.1.6 Cysteine *i, i+4* stapling with *1,3-bis(bromomethyl)benzene* – general protocol

Lyophilized Mizmetic 1-22 (1 eq., 10 mM) and 1,3-bis(bromomethyl)benzene (1 eq., 10 mM) were dissolved in 80% NH_4HCO_3 buffer (100 mM, pH = 8) containing 20% MeCN and let to react for 30 minutes at RT. The reaction was stopped by flash freezing in liquid nitrogen followed by lyophilization or, alternatively, the mixture was directly purified according to the general purification protocol.

5.5.1.7 LC-MS

LC-MS spectra were obtained with a Shimazu LCMS-2020 system (Method A) equipped with a Kinetex® 2.6µm XB-C18 100 Å LC Column (50 x 3 mm) and UV detector set to 214 nM. High resolution LC-MS spectra were obtained with a Sciex X500b QTOF ESI-QToF mass spectrometer coupled to a Shimadzu Nexera UHPLC LC40DX3 (Method B) equipped with a Phenomenex Synergi™ 4 µm Fusion-RP 80 Å LC Column (50 x 2 mm) or Aeris™ 3.6 µm Widepore XB-C18 set to 214 nM. For both Method A and Method B the solvent phases used were solvent A (0.1% formic acid in water) and solvent B (0.1% formic acid in MeCN).

Method A:

Column: Kinetex® 2.6µm XB-C18 100 Å LC Column (50 x 3 mm) UV detector: 214 nm.

LC Method: 0% solvent B for 1 min, 0% to 70% solvent B over 10 min 70% solvent B over 1.5 min, 70% to 0% solvent B over 4.5, flowrate 0.55 mL/min.

Method B (High resolution):

Column: Phenomenex Synergi™ 4 µm Fusion-RP 80 Å LC Column (50 x 2 mm) or Aeris™ 3.6 µm Widepore XB-C18.

LC Method: 0% solvent B for 1 min, 0% to 90% solvent B over 6 min, 90% solvent B

over 2 min, 90% to 0% solvent B over 0.5 min, 0% solvent B over 1.5 min, flowrate 0.5 mL/min.

MS parameters: General parameters: Method duration: 5 min; Total scan time: 0.276 sec; Estimated cycles: 1086; Intact protein mode: False; Decrease detector voltage: False; Large protein (>70 kDa): False; Ion Source: Source name: TurbolonSpray; Curtain gas: 35 psi; Ion source gas 1: 60 psi; Ion source gas 2: 60 psi; Temperature: 500 ˚C; Experiment: Scan type: TOF MS; Polarity: Positive; Spray voltage: 5500 V; CAD gas: 7; Time bins to sum: 4; Channel 1-4: True; TOF start mass: 350 Da; TOF stop mass 1500 Da; Accumulation time: 0.25; Declustering potential: 80V; Declustering potential spread: 0 V; Collision energy: 10V; Collision energy spread: 0 V; Override Qjet RF value: False

5.5.2 Protein synthesis with LCMS spectra

5.5.2.1 Fluorescent labeling of MYC (MYC_F)

Dulbecco's Phosphate buffered saline (DPBS, pH = 6.75) was degassed using a gentle nitrogen stream for 15 minutes. MYC (2.28 mg, 143.7 nmol, 1 eq.) was dissolved in H_2O (228 µL, 10 mg/mL). A 10 mg/mL stock solution of N-(5-Fluoresceinyl) maleimide in DMSO was prepared. The complete MYC solution, was mixed with 6.14 µL of N-(5-Fluoresceinyl)maleimide stock (0.06 mg, 143.7 nmol, 1 eq.) and 905.9 µL degassed buffer resulting in a final concentration of 2 mg/mL of MYC and 0.05 mg/mL N-(5-Fluoresceinyl)maleimide. The reaction was quenched by flash freezing in liquid nitrogen followed by lyophilization after 15 minutes and purified on a Biotage® Selekt Flash Purification System equipped with a Biotage® Sfär C18 D - Duo 25g column using UV detection at 214 nm with H_2O + 0.1% TFA (Buffer A) and MeCN+0.1% TFA (Buffer B). The following gradient was used: 0% buffer B for 2 CV, 0% to 80% buffer B over 11.4 CV, 95% Buffer B for 2 CV. The combined fractions containing the protein were lyophilized, yielding the protein as TFA salt. Yield: 1.47 mg, 72.5 nmol, 50%

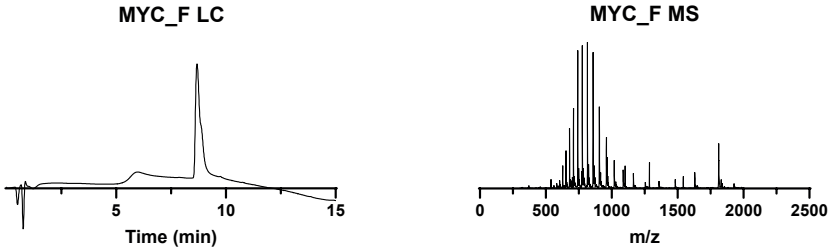

UV LC-MS trace of MYC_F. LC-MS trace was obtained with Method A.

5.5.2.2 Fluorescent labeling of His-tagged MAX (MAX_F)

DPBS (pH = 6.75) was degassed using a gentle nitrogen stream for 15 minutes. MAX (7.97 mg, 524.2 nmol, 1 eq., MAX) was dissolved in H_2O (797 µL, 10 mg/mL). A 10 mg/mL stock solution of N-(5-Fluoresceinyl)maleimide in DMSO was prepared. MAX, was mixed with 22.4 µL of N-(5-Fluoresceinyl)maleimide stock (0.22 mg, 524.2 nmol, 1 eq.) and 3165.5 µL degassed buffer resulting in final concentration of 2 mg/mL of MAX and 0.06 mg/mL N-(5-Fluoresceinyl)maleimide. The reaction was quenched by flash freezing in liquid nitrogen followed by lyophilization after 30 minutes and purified on a Biotage® Selekt Flash Purification System equipped with a Biotage® Sfär C18 D - Duo 25 g column using UV detection at 214 nm with H_2O + 0.1% TFA (Buffer A) and MeCN+0.1% TFA (Buffer B). The following gradient was performed: 0% buffer B for 3 CV, 0% to 30% buffer B over 4.3 CV, 30% to 70% buffer B over 5.7 CV, 95% Buffer B for 2 CV. The combined fractions containing the protein were lyophilized, yielding the protein as TFA salt. Yield: 3.64 mg, 220 nmol, 67%

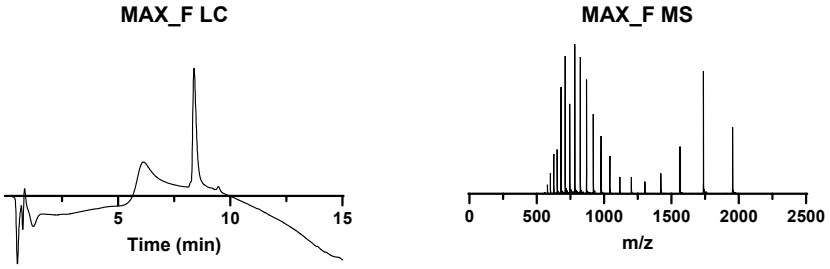

UV LC-MS trace of MYC_F. LC-MS trace was obtained with Method A.

5.5.2.3 Mizmetic peptides

All Mizmetic peptides were synthesized according to the protocols described in Supplemental info 2.1 -2.6. Yields can be found in section 5.1 and LC-MS traces can be found in section 7.1. All Mizmetic peptides were stored as a 1 mM solution in pure DMSO.

5.5.3. Biochemistry

5.5.3.1. Overview of buffers used

MYC Bacterial cell lysis buffer	20mM HEPES, pH 8, 0.5 M NaCl, 3mM $MgCl_2$, 0.05% DNAse, complete EDTA free protease inhibitor (1 tablet freshly added in 50 mL buffer)
MAX Bacterial cell lysis buffer	20 mM Tris-HCl, pH 8, 0.5 M NaCl, 3mM $MgCl_2$, 0.05% DNAse, complete EDTA free protease inhibitor (1 tablet freshly added in 50 mL buffer)
MYC extraction buffer	20 mM HEPES, 6M Gdn HCl, 0.5 M NaCl, 10 mM imidazole, pH = 8
MYC affinity wash buffer	20 mM HEPES, 6M urea, 0.5 M NaCl, 10 mM imidazole, pH = 8
MYC affinity elution buffer	20 mM HEPES, 6M urea, 0.5 M NaCl, 500 mM imidazole, pH = 8
MAX affinity wash buffer	20 mM Tris-HCl, 0.5 M NaCl, 10mM imidazole, pH = 8
MAX affinity elution buffer	20 mM Tris-HCl, 0.5 M NaCl, 500mM imidazole, pH = 8
EMSA loading buffer	20 mM HEPES, 100 mM NaCl, 5% glycerol, 1 mM EDTA, 20 mM $MgCl_2$, 1 mM DTT and 0.02% Tween-20, pH = 7
EMSA running buffer	25 mM Tris-HCl, 192 mM Glycine, pH = 8.3
BLI kinetic buffer	10 mM HEPES, 50 mM NaCl, 0.02% Tween-20, 0.1% BSA, pH = 7.4

5.5.3.2. Expression of MYC and MAX in E.Coli

Performed as described elsewhere.[1] pET-30 plasmid with His-tagged $MYC_{369-454}$ (Uniprot entry P01106) or His-tagged MAX were transformed into competent ArcticXpress DE3 RIL cells (Agilent) according to suppliers manual. All LB medium used was supplemented with kanamycin and gentamycin. Single colonies were cultured overnight at 37 °C and 200 rpm in 100 mL LB medium. Overnight culture was evenly distributed over 3x2L erlenmeyer flasks (total volume 6L) and allowed to reach an OD of 0.8 at 37 °C and 200 rpm. Then, temperature was cooled down to 14 °C before 100 µM IPTG was administered. After 18 hours, cells were harvested by centrifugation at 4 °C and 5000g for 12 minutes. Then, cell pellet was lysed with pressure lysis and lysis buffer (see overview of buffers 5.1). Lastly, cell debris, when MYC was expressed including inclusion bodies, was separated from supernatant by centrifugation at 4 °C and 50.000g for 45 minutes.

5.5.3.3. Purification of His-tagged MAX (MAX)

The supernatant after ultracentrifugation was purified using an ÄKTA start protein purification system attached to a 5 mL HisTrap HP His-tag protein purification column (Cytiva). Unbound protein was allowed to flow through at 100% wash buffer (see

Supplementary 5.1) before MAX was eluted with elution buffer (see Supplementary 5.1) over 40-50 CV. Pure fractions were analyzed by LC-MS method B.

5.5.3.4. Purification of His-tagged MYC (MYC) from inclusion bodies

The ultracentifuge pellet was first washed with 2M urea in Buffer A (500 mM NaCl, 20 mM HEPES, 10 mM imidazole, pH=8), then 1% Triton x-100 in buffer A and lastly with 1M NaCl in Buffer A following an extraction in 40 mL of extraction buffer (6M Gdn HCl, 500 mM NaCl, 20 mM HEPES, 10 mM imidazole, pH=8) and left overnight at 4 °C while rotating. The mixture was then centrifuged for 30 min at 10.000g and the supernatant was collected and stored at 4 °C for later use. The pellet was then again incubated in 15 mL of extraction buffer and stirred for 16h at RT followed by centrifugation for 30 min at 10.000g. The supernatant was collected and combined with the previously obtained supernatant. Next, the supernatant was loaded onto an Äkta pure purification system equipped with a 5 mL HisTrap HP His-tag protein purification column (Cytiva) that was primed with the extraction buffer with 4 mL/min. The system was subsequently washed with 20 mL of buffer A (20 mM HEPES, 6M urea, 500 mM NaCl, 10 mM imidazole, pH = 8) followed by a gradient of 10-250mM imidazole Buffer B (20 mM HEPES, 6M urea, 500 mM NaCl, 500 mM imidazole, pH = 8) over 30 CV. The system was then washed with 20 mL of 500mM imidazole Buffer B. All fractions where stored at -80 °C when not directly used and analyzed by SDS-PAGE and LC-MS.

5.5.3.5. Protocol for buffer exchange His-MAX (MAX)

Pure fractions were incubated with 0.5-1 mM TCEP for 1 hour before buffer exchange was performed with a Biotage® Selekt Flash Purification System attached to a Biotage® Sfär C18 D - Duo 25g or 50g column using UV detection at 214 nm. A stepwise gradient was performed with 100% H_2O (with 0.1% TFA) to 50% in MeCN (with 0.1% TFA), to 100% MeCN (with 0.1% TFA). Fractions were analyzed with LC-MS, combined and lyophilized yielding His-MAX as TFA salt.

5.5.3.6. Protocol for buffer exchange His-MYC (MYC)

Pure fractions were combined and buffer exchange was performed using reverse phase chromatography using a Biotage Selekt attached to a Biotage® Sfär Bio C18 D Duo 300 Å 20 µm 50g column using UV detection at 214 nm with H_2O +0.1% TFA (solvent A) and MeCN+0.1% TFA (Solvent B). The following gradient was performed: 0%B for 5CV, then 50%B for 4CV, then 100%B for 3 CV. Fractions were analyzed with LC-MS, combined and lyophilized. An unknown post translational modification was observed for MYC with an extra mass of +75. MYC was incubated with 100 eq. TCEP in H_2O for 2 hours at RT and buffer exchange was performed using the same protocol. The combined fractions containing the protein were lyophilized, yielding

the His-tagged protein as TFA salt.

5.5.3.7. General protocol for SDS-PAGE

Fractions from protein purification were 10-1000x diluted and mixed with 4x Laemmli buffer with β-mercaptoethanol. Samples were incubated 5 minutes for 95 °C, loaded on a 12.5% acrylamide gel (prepared with acrylamide 37.5:1 acrylamide/Bis) and ran for 45 minutes at 200 V at RT. Then, gel was stained with Coomassie blue for 1h or overnight and 3x destained for at least 15 minutes with refreshed destaining solution (50% MeOH, 40 % H_2O, 10% AcOH). Gels were analyzed with a Bio-Rad ChemiDoc MP machine.

5.5.3.8 Biolayer interferometry (BLI)

All Mizmetic compounds where directly diluted from their stock solution to 50 nM solution in kinetic buffer (10 mM HEPES, 50 mM NaCl, 0.02% Tween-20, 0.1% BSA, pH = 7.4) and screened against MYC in kinetic buffer. For a concentration curve MYC was stepwise diluted in kinetic buffer. To obtain an affinity for Mizmetic WT, the average of three separate measurements was calculated, screened against 5 µM MYC and the background removed. The following protocol was performed for a standard BLI assay:

The streptadavin coated tips where first soaked in kinetic buffer for at least 10 minutes, while the 96 well plate was shaking at 1000 rpm and 37 °C. The following steps were performed: baseline step (1 min), Mizmetic loading step (3 min), washing step (1 min), additional separate washing step (1 min), association step (5 min), dissociation step (5 min). All steps where performed at 37 °C while shaking at 1000 rpm. After measurement, the background measurement performed was without peptides loaded on the tips against the same MYC concentration and these background traces were subtracted. Fitting and kinetic K_Ds calculations were performed with the provided Sartorius Octed software. An Sartorius Octet R4 was used for the assay. The graph was plotted using GraphPad Prism 10.1.0.

5.5.3.9 Circular Dichroism (CD)

Lyophilized Mizmetic peptides were dissolved to 50 µM (Mizmetic 1C and 2) or 100 µM (Mizmetic WT) in 200 µL Tris acetate buffer (10 mM Tris acetate, 50 mM NaCl, pH = 7.4) and measured with a Jasco J-815 machine. Samples were measured in a High Precision Cell quartz cuvette (Hellma Analytics) with 1 mm Pathlength at 37 °C. Then, 10 µM of MYC was added to the same sample. Mizmetic and MYC were incubated in the machine for 10 minutes at 37 °C before measurement. The following CD parameters were utilized: start 260 nm, end 200 nm, Sensitivity standard, D.I.T. 1 sec., Data pitch 1 nm, scanning mode continuous, scanning speed 100 nm/min,

accumulations 5. The background was removed for all spectra. Spectra with MYC and Mizmetics were normalized twice, first for Mizmetic, second for MYC. The average values were used to portray the CD spectra. % helicity was calculated using the BestSEL software tool. [2,3] To calculate % helicity for Mizmetics together with MYC helicity was calculated normalized to both Mizmetic and MYC. The average value is reported. Spectra's were normalized according to the following formula:[4]

$$\left[\emptyset\right] = \frac{100*\emptyset_{obs}}{c*n*l}$$

With θ in deg*cm^{2}*dmol^{-1}, θ_{obs} in mdeg, concentration (c) in mM, peptide bonds (n) and path length of cuvette in cm. The graph was plotted using GraphPad Prism 10.1.0.

5.5.3.10 Truncation comparison of Mizmetics

The general BLI protocol was performed, screened against 300 nM MYC. After subtraction of the background, the KD was calculated and the KD compared to Mizmetic 1**.** The graph was plotted using GraphPad Prism 10.1.0.

5.5.3.11 Alanine scan comparison of Mizmetics

For the alanine scan the general BLI protocol was performed, screened against 400 nM MYC. After subtraction of the background, the KD was calculated and the relative KD compared to Mizmetic 2 in the same assay was plotted in a barplot using GraphPad Prism 10.1.0. Following formula was used to calculate relative KD.

$$\left[Relative\ \ K_D\right] = \frac{K_{D\ \ Mizmetic\ \ 2}}{K_{D\ \ variants}} * 100\,\%$$

5.5.3.12 General protocol for competition assay with labeled DNA

5x 7.5% native gels were prepared using 7.5 mL 30% Acrylamide/Bis solution (19:1 with 5% crosslinker), 7.5 mL 1.5M Tris pH = 8.8, 15 mL H_2O, 30 µL TEMED and 150 µL 10% APS. Mizmetic peptides were diluted to 40 µM in 1x loading buffer (20 mM HEPES, 100 mM NaCl, 5% glycerol, pH = 7, 20 mM $MgCl_2$, 1 mM DTT, 0.02% Tween-20, see Supplemental 5.1), MYC/MAX were separately diluted to 60 nM in 1x loading buffer. Labelled DNA construct (IRD700-ACC CCA C**CA CGT G**GT GCC T) was first incubated at 95 °C for 5 min, cooled down and diluted to 16 nM (4x) in 1x loading buffer. Next, 5 µL of 4x Mizmetic was incubated while shaking at RT with 5 µL of 4x MYC. MYC was also in a separate lane incubated with 200 µM 10058-F4, a known MYC/MAX inhibitor.[5] After 1h, 5 µL of 4x MAX and 5 µL labeled DNA construct were added to each well resulting in the following concentrations: Mizmetic 10 µM, MYC 15 nM, MAX 15 nM, DNA 4 nM, DMSO 1%. Lanes always contained

≤1% DMSO. This solution was incubated for 5 min at RT while shaking followed by placement on ice while loading 12.5 µL onto the gel which was pre-run before for 1h at 100V at 4 °C in 1x running buffer (25 mM Tris-HCl, 192 mM Glycine, pH = 8.3). Samples ran for 80 minutes at 75V at 4 °C. Gels were rinsed with demi water and DNA was visualized with Bio-Rad ChemiDoc MP machine.

5.5.3.13 General protocol for competition assay with labeled MYC (MYC_F) or MAX (MAX_F)

The standard protocol described in 4.13 was followed. For MYC labeled gels, MYC_F and MAX were separately diluted to 60 nM in 1x loading buffer. For MAX labeled gels, MAX_F was diluted to 120 nM in 1x loading buffer. The following unlabeled DNA hairpin construct was used: TTC CT**C ACG TG**G CAT TTG GGT GC**C ACG TG**A GG. MYC_F or MAX_F was visualize with a Bio-Rad ChemiDoc MP machine. Next, gels were incubated with SYBR Gold (1:50.000 in running buffer) for 5-40 minutes and again visualized with the Bio-Rad ChemiDoc MP machine. Lanes always contained ≤1% DMSO.

For a concentration curve, the Mizmetic peptide was first stepwise diluted in DMSO followed by a further dilution in loading buffer (20 mM HEPES, 100 mM NaCl, 5% glycerol, pH = 7, 20 mM $MgCl_2$, 1 mM DTT, 0.02% Tween-20) to a 4x concentration. The assay was performed with following final concentrations: Mizmetic 10-0.1 µM**,** MYC_F 15 nM, MAX 15 nM, DNA 40 nM or Mizmetic 10-0.1 µM**,** MAX_F 30 nM, DNA 40 nM. Gels were quantified with ImageJ 1.54f. For MYC gels the intensity of free MYC was removed from each lane. IC_{50} was calculated using GraphPad Prism 10.1.0 with the Nonlinear Regression One site – Fit logIC50 analysis. All concentration curves were performed in at least duplicates.

5.5.4 AlphaFold-Multimer inputs

MID1-MYC	
MID1:	EESAGTDSGQELGSEARGLRSGTYGDRTESKAYGSVIHKC
MYC:	GHMNVKRRTHNVLERQRRNELKRSFFALRDQIPELENNEKAPKVVILK-KATAYILSVQAEEQKLISEEDLLRKRREQLKHKLEQLGGC

MID2-MYC	
MID2:	HQGKAGIKILEPEEGSEVSVVTVDDMVTLATEALAATAVTQLTVVPV-GAAVTADETEVLKAEISKAVKQVQEEDPNTHILYA
MYC:	GHMNVKRRTHNVLERQRRNELKRSFFALRDQIPELENNEKAPKVVILK-KATAYILSVQAEEQKLISEEDLLRKRREQLKHKLEQLGGC

Mizmetic WT - MYC	
Mizmetic WT:	AAVTADETEVLKAEISKAVKQVQEEDPN
MYC:	GHMNVKRRTHNVLERQRRNELKRSFFALRDQIPELENNEKAPKVVILK-KATAYILSVQAEEQKLISEEDLLRKRREQLKHKLEQLGGC

Mizmetic Zinc mutant - MYC	
Mizmetic:	AAVTADETEVLKAEICKAVCQVQEEDPN
MYC:	GHMNVKRRTHNVLERQRRNELKRSFFALRDQIPELENNEKAPKVVILK-KATAYILSVQAEEQKLISEEDLLRKRREQLKHKLEQLGG
Ion	Zinc

5.5.5 Supporting Tables

Supporting table 5.1: All compounds with corresponding sequence, stapling, calculated mass, found mass and yield. Yield is reported over peptide synthesis and stapling.

Compound #		Sequence (N –> C)	Stapled	m/z calc.	m/z found	Yield (%)	Yield (mg)	Yield (µmol)
WT	NH_2	K(Biotin)A$_\beta$AAVTADETEVLKAEISKAVKQVQEEDPN	No	3437.87	3437.8	4	5.51	1.6
1	Ac	AAVTADETEVLKAEICKAVCQVQEEDPNA$_\beta$K(Biotin)	Yes	3573.07	3572.1	1.5	1.1	0.9
2	Ac	----ADETEVLKAEICKAVCQVQEEDPNA$_\beta$K(Biotin)	Yes	3230.67	3229.8	1.9	2.5	0.4
3	Ac	----ADETEVLKAEICKAVCQVQE----A$_\beta$K(Biotin)	Yes	2775.25	2774.9	1.3	0.72	0.3
4	Ac	----ADETEVLKAEICKAVCQVQEEDPAA$_\beta$K(Biotin)	Yes	3187.65	3187.4	6.7%	2.21	0.7
5	Ac	----ADETEVLKAEICKAVCQVQEEDANA$_\beta$K(Biotin)	Yes	3204.64	3204.4	5.9%	1.96	0.6
6	Ac	----ADETEVLKAEICKAVCQVQEEAPNA$_\beta$K(Biotin)	Yes	3186.67	3186.5	9.2%	3.02	0.9
7	Ac	----ADETEVLKAEICKAVCQVQEADPNA$_\beta$K(Biotin)	Yes	3172.64	3172.4	5.8%	1.9	0.6
8	Ac	----ADETEVLKAEICKAVCQVQAEDPNA$_\beta$K(Biotin)	Yes	3172.64	3172.4	7.2%	2.39	0.8
9	Ac	----ADETEVLKAEICKAVCQVAEEDPNA$_\beta$K(Biotin)	Yes	3173.62	3173.4	6.7%	2.22	0.7
10	Ac	----ADETEVLKAEICKAVCQAQEEDPNA$_\beta$K(Biotin)	Yes	3202.62	3202.4	12.2%	4.02	1.3
11	Ac	----ADETEVLKAEICKAVCAVQEEDPNA$_\beta$K(Biotin)	Yes	3173.62	3173.4	7.6%	2.52	0.8
12	Ac	----ADETEVLKAEICKAACQVQEEDPNA$_\beta$K(Biotin)	Yes	3202.62	3202.0	9.7%	3.2	1
13	Ac	----ADETEVLKAEICAAVCQVQEEDPNA$_\beta$K(Biotin)	Yes	3173.58	3173.2	0.6%	0.2	0.06
14	Ac	----ADETEVLKAEACKAVCQVQEEDPNA$_\beta$K(Biotin)	Yes	3188.59	3188.3	3.4%	1.12	0.4
15	Ac	----ADETEVLKAAICKAVCQVQEEDPNA$_\beta$K(Biotin)	Yes	3172.64	3172.2	1.7%	0.55	0.2
16	Ac	----ADETEVLAAEICKAVCQVQEEDPNA$_\beta$K(Biotin)	Yes	3173.58	3173.2	0.7%	0.98	0.3
17	Ac	----ADETEVAKAEICKAVCQVQEEDPNA$_\beta$K(Biotin)	Yes	3188.59	3188.3	1.4%	0.46	0.1
18	Ac	----ADETEALKAEICKAVCQVQEEDPNA$_\beta$K(Biotin)	Yes	3202.62	3202.4	4.9%	1.6	0.5
19	Ac	----ADETAVLKAEICKAVCQVQEEDPNA$_\beta$K(Biotin)	Yes	3172.64	3172.4	0.4%	0.14	0.04
20	Ac	----ADEAEVLKAEICKAVCQVQEEDPNA$_\beta$K(Biotin)	Yes	3200.65	3200.4	3.7%	1.22	0.4
21	Ac	----ADATEVLKAEICKAVCQVQEEDPNA$_\beta$K(Biotin)	Yes	3172.64	3172.5	3.6%	0.12	0.04
22	Ac	----AAETEVLKAEICKAVCQVQEEDPNA$_\beta$K(Biotin)	Yes	3186.67	3186.5	1.5%	0.49	0.2

Supporting table 5.1: All compounds with corresponding sequence, stapling, calculated mass, found mass and yield. Yield is reported over peptide synthesis and stapling.

Compound #		Sequence (N –> C)	Stapled	m/z calc.	m/z found	Yield (%)	Yield (mg)	Yield (µmol)
His-MYC (MYC)	NH_2	MHHHHHHSSGLVPRGSGMKETAAAKFERQHMD-SPDLGTDDDDKAMADIGSNVKRRTHNVLERQRR-NELKRSFFALRDQIPELENNEKAPKVVILKKATAY-ILSVQAEEQKLISEEDLLRKRREQLKHKLEQLRNSCA	N.A	15865.82	15865.5	N.A	N.A	N.A
MYC_F	NH_2	MHHHHHHSSGLVPRGSGMKETAAAKFER-QHMDSPDLGTDDDDKAMADIGSNVKRRTH-NVLERQRRNELKRSFFALRDQIPELEN-NEKAPKVVILKKATAYILSVQAEEQKLI-SEEDLLRKRREQLKHKLEQLRNSC(FITC)A	N.A	16293.4	16292.7	50	1.47	0.07
His-MAX (MAX)	NH_2	MHHHHHHSSGLVPRGSGMKETAAAKFERQHMD-SPDLGTDDDDKAMADIGSDKRAHHNALERKRRD-HIKDSFHSLRDSVPSLQGEKASRAQILDKATEYIQYM-RRKNHTHQQDIDDLKRQNALLEQQVRALGGC	N.A	15203.71	15203.5	N.A	N.A	N.A
MAX_F	NH_2	MHHHHHHSSGLVPRGSGMKETAAAKFERQHMD-SPDLGTDDDDKAMADIGSDKRAHHNALERKRRD-HIKDSFHSLRDSVPSLQGEKASRAQILDKATEYIQYMR-RKNHTHQQDIDDLKRQNALLEQQVRALGGC(FITC)	N.A	15631.27	15630.8	67	3.64	0.2

Supporting table 5.2: Observed affinities according to BLI for Mizmetic WT and Mizmetic 1 analogues.

Mizmetic #	KD (μM)	KD (nM)	Times difference compared to WT
WT	4.599	4599.2	1
1	0.176	176	26

Supporting table 5.3: Observed affinities according to BLI for Mizmetic 1 and truncated peptides. Percentages where calculated by dividing the affinity by the affinity of Mizmetic 1.

Mizmetic #	KD (nM)	Times difference compared to WT
1	119.8	1
2	118.6	1
3	6007.4	50

Supporting table 5.4 Observed affinities according to BLI for all Mizmetic 2 analogues compared to Mizmetic 2.

Mizmetic #	KD (nM)	Relative KD (%)
2	115.56	100%
4	118.72	97%
5	134.58	86%
6	159.91	72%
7	233.12	50%
8	167.29	69%
9	131.59	88%
10	184.54	63%
11	121.60	95%
12	529.56	22%
13	98.29	118%
14	1075.83	11%
15	161.49	72%
16	108.00	107%
17	38182.51	0%
18	146.00	79%
19	109.64	105%
20	99.49	116%

Supporting table 5.4 Observed affinities according to BLI for all Mizmetic 2 analogues compared to Mizmetic 2.

Mizmetic #	KD (nM)	Relative KD (%)
21	77.25	150%
22	171.03	68%

5.5.6 Supporting Figures

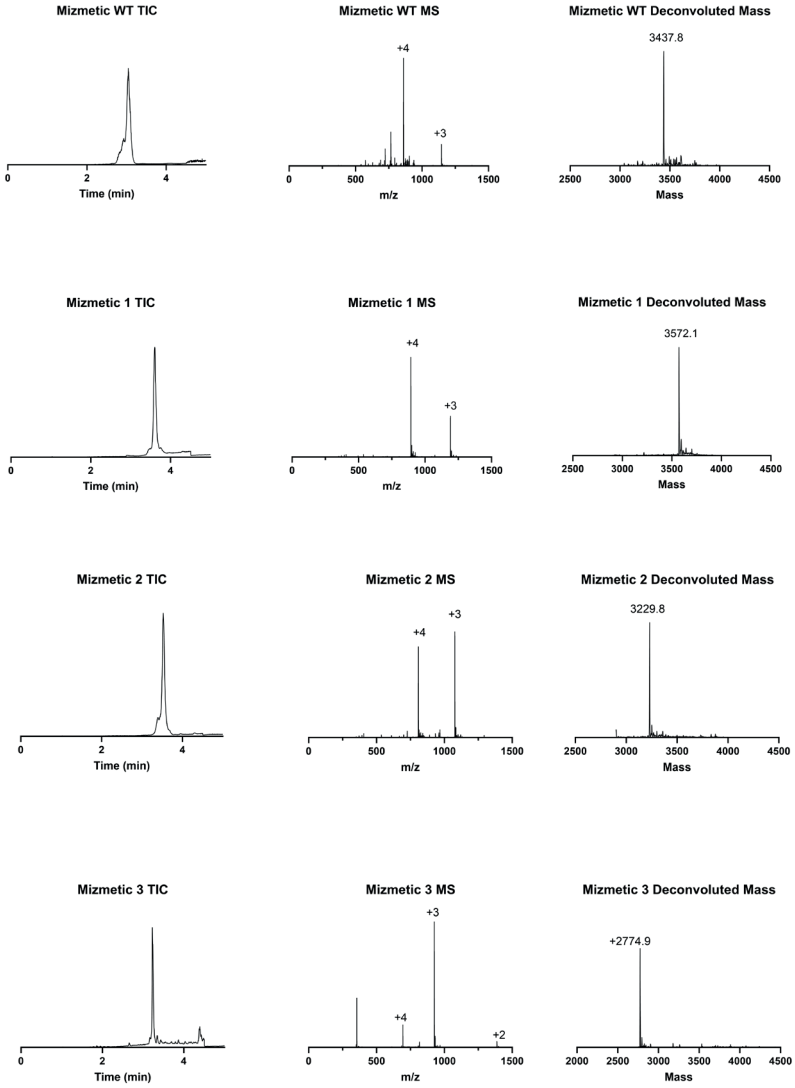

▲**Figure S5.1:** LC-MS traces of Mizmetic WT and 1-3. LC-MS traces were obtained with Method B.

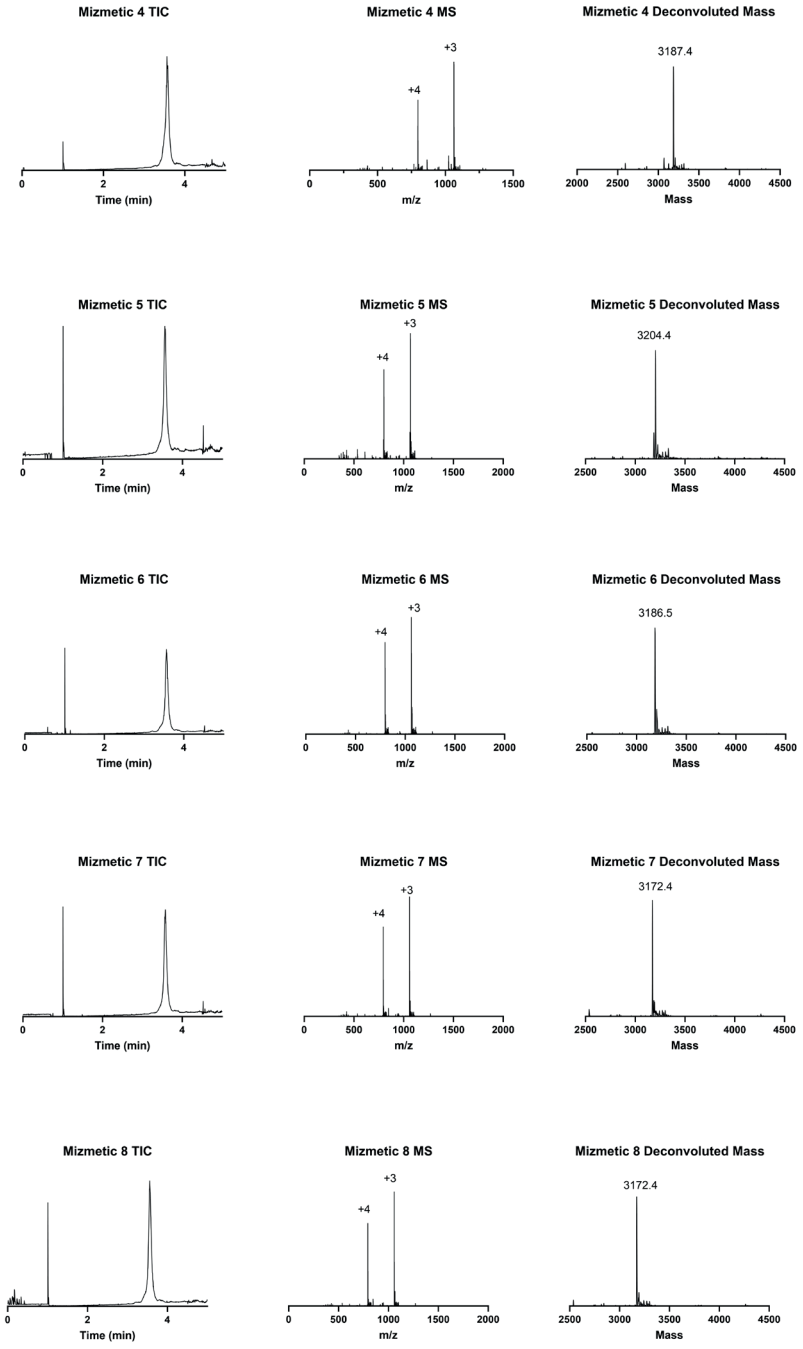

▲**Figure S5.2:** LC-MS traces of Mizmetic 4-8. LC-MS traces were obtained with Method B.

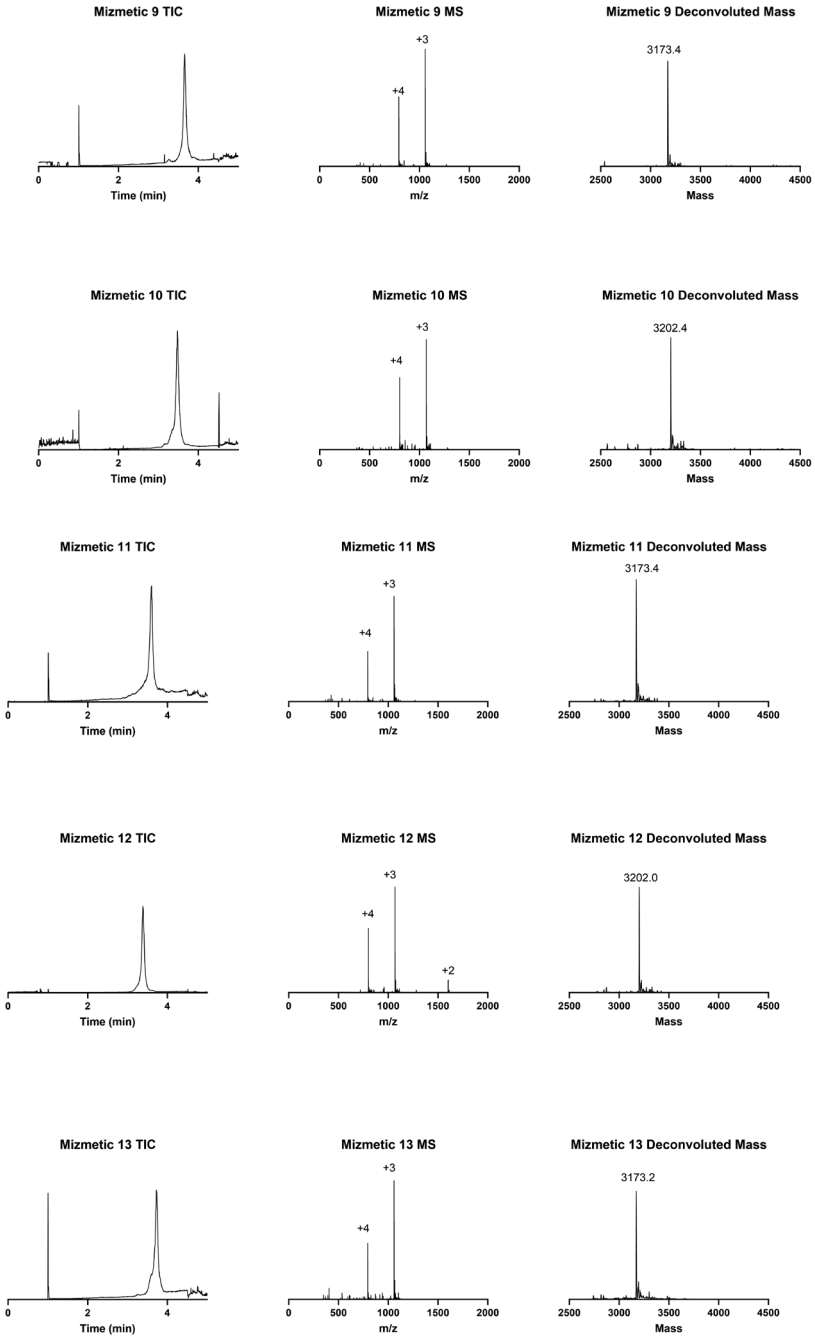

▲**Figure S5.3:** LC-MS traces of Mizmetic 9-13. LC-MS traces were obtained with Method B.

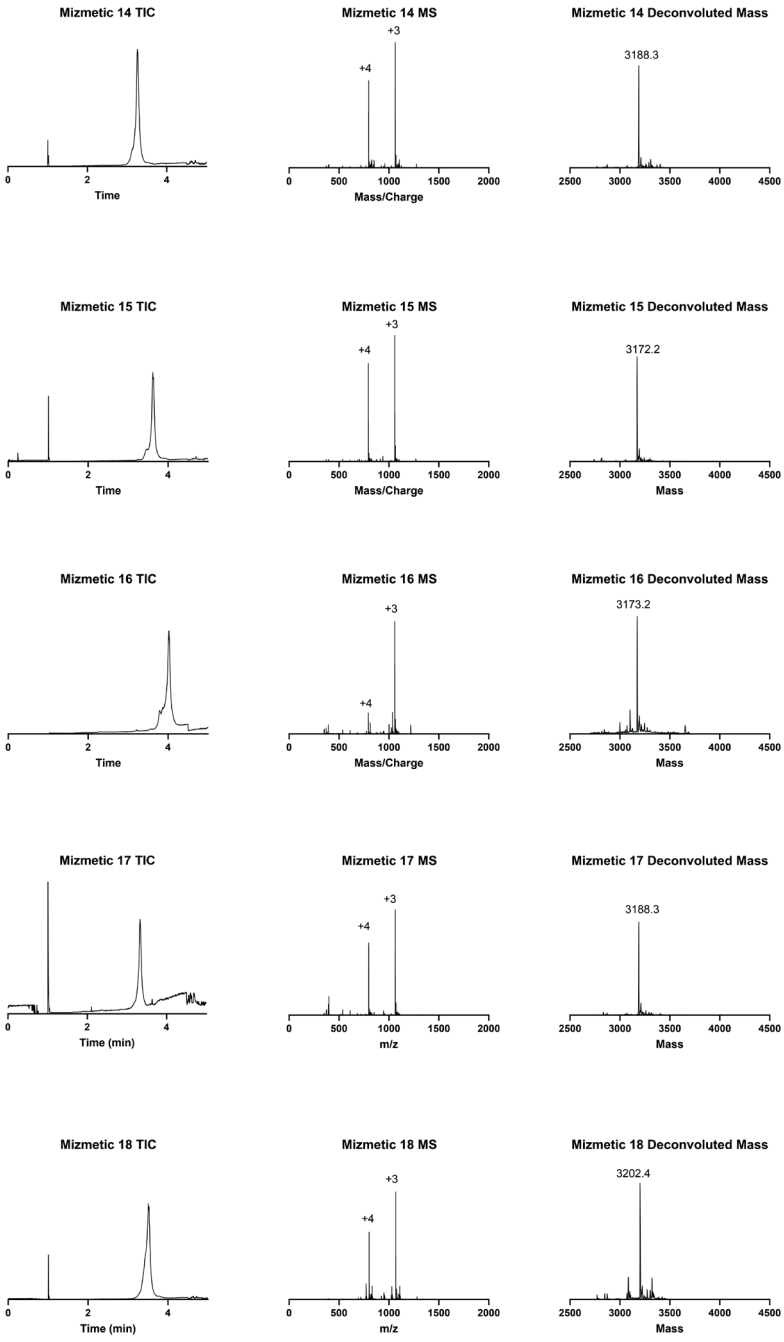

▲**Figure S5.4:** LC-MS traces of Mizmetic 14-18. LC-MS traces were obtained with Method B.

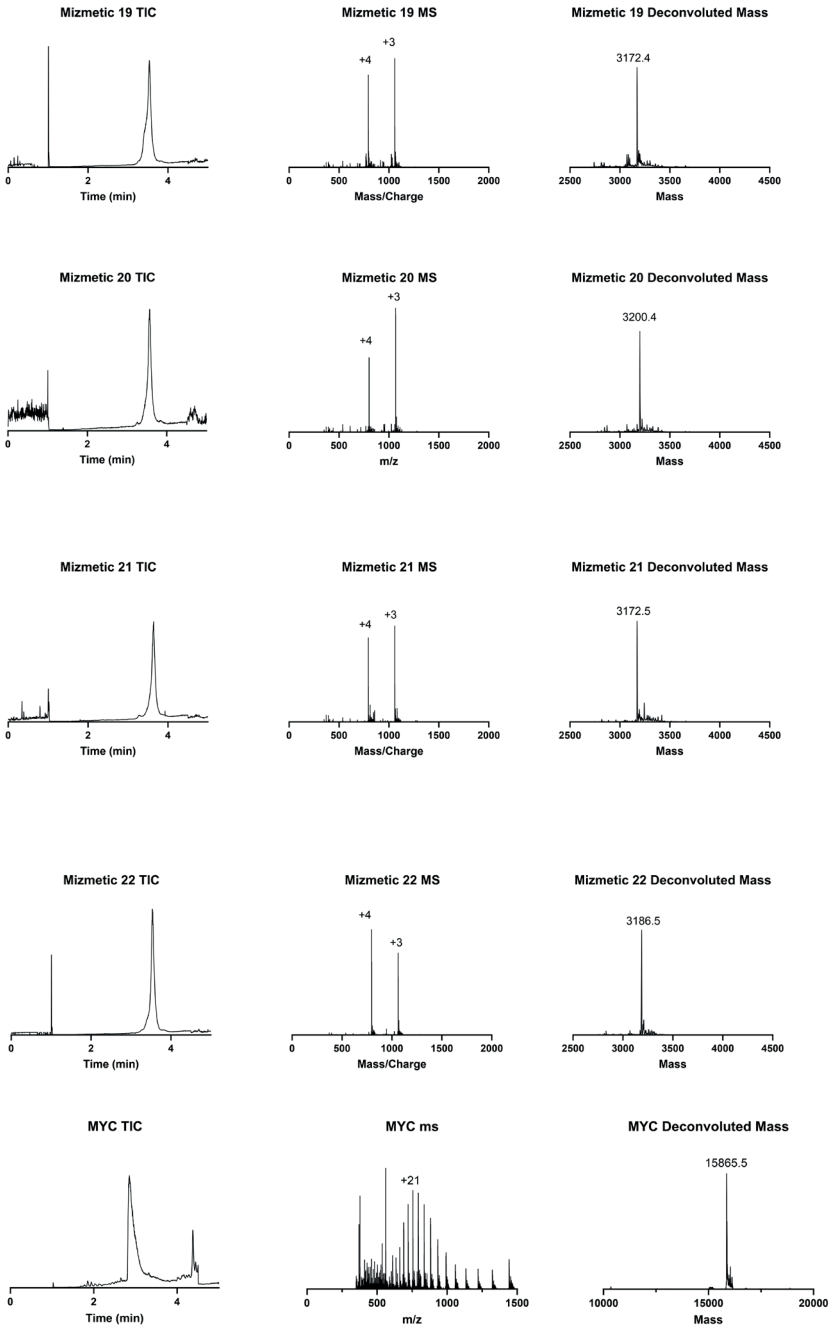

▲**Figure S5.5** LC-MS traces of Mizmetic 19-22, Myc and Myc-F. LC-MS traces were obtained with Method B.

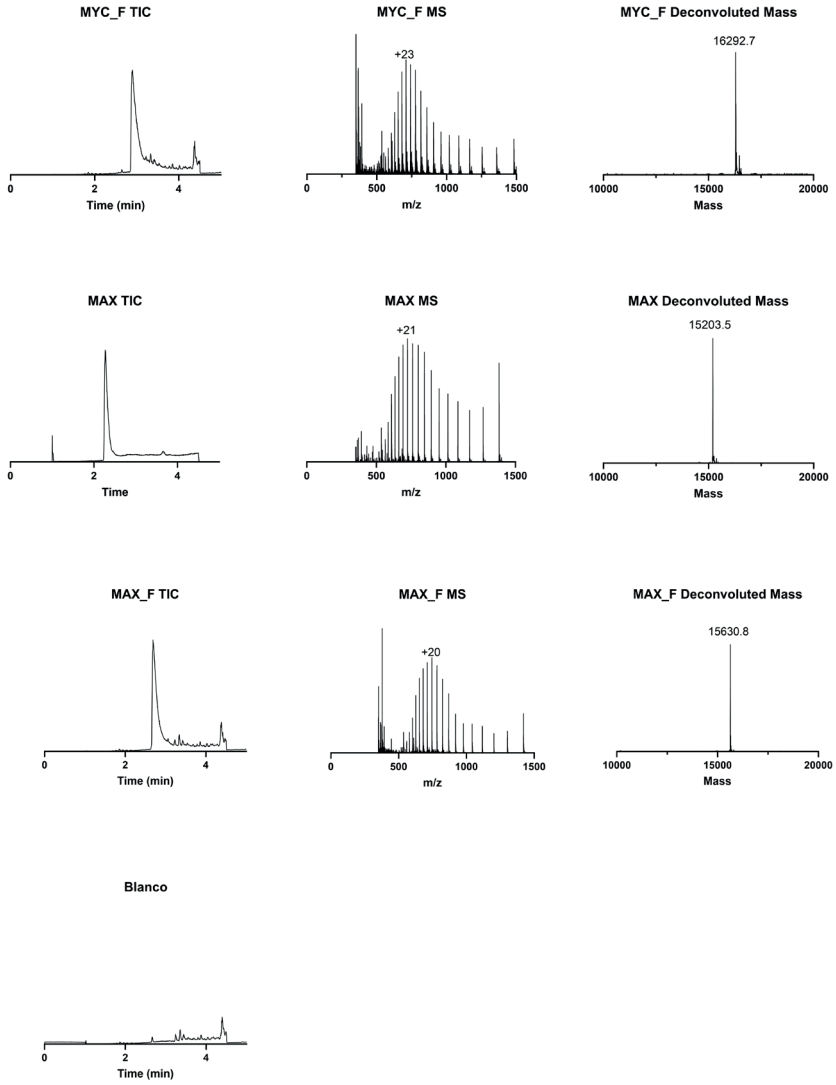

▲**Figure S5.6** LC-MS traces of MAX, Max-F and the blanco measured at the same day as MYC, MYC_F, MAX_F, Mizmetic 3. LC-MS traces were obtained with Method B.

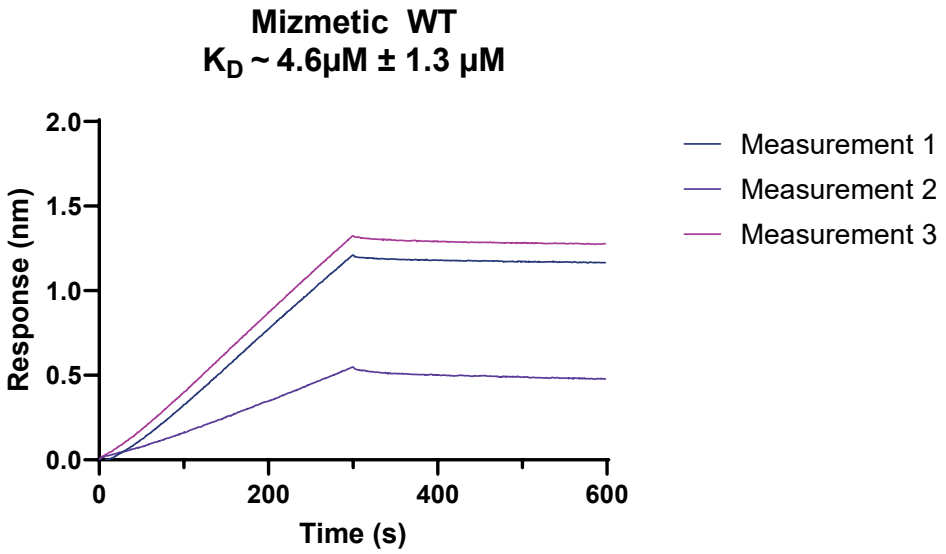

▲Figure S5.7: BLI curves show that Mizmetics have affinity towards MYC. Mizmetic WT displays an affinity of 4.6 μM ± 1.3 μM according to three independent BLI curves screened against 5 μM MYC.

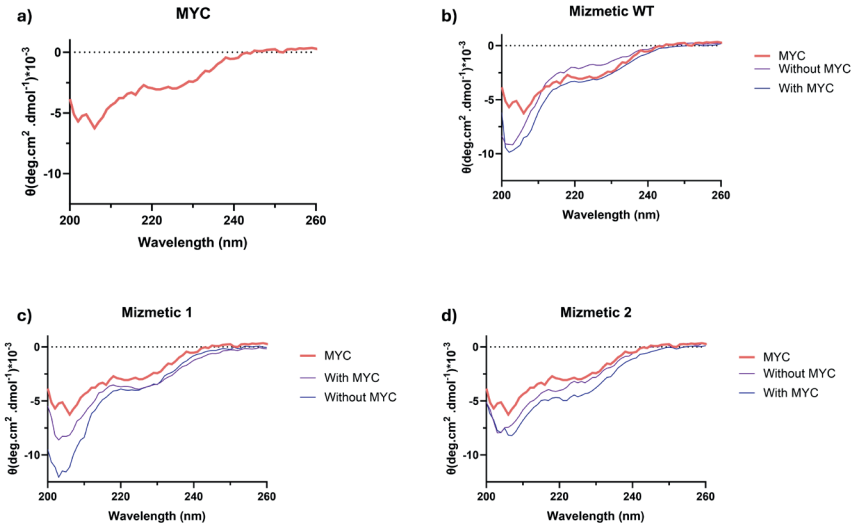

▲Figure S5.8: All Mizmetics display a partial α-helix with or without the presence of MYC. a) CD spectrum of MYC without a Mizmetic. b) CD spectrum of Mizmetic WT with or without MYC. c) CD spectrum of Mizmetic 1 with or without MYC. d) CD spectrum of Mizmetic 2 with or without MYC. Lyophilized Mizmetics were diluted to 50 μM in 200 μL Tris acetate buffer (10 mM Tris acetate, 50 mM NaCl, pH = 7.4) with a Jasco J-815 at 37 °C. After the initial measurement, 10 μM MYC was added to the same cuvette and the cuvette was incubated for 10 minutes inside the machine at 37 °C before measurement.

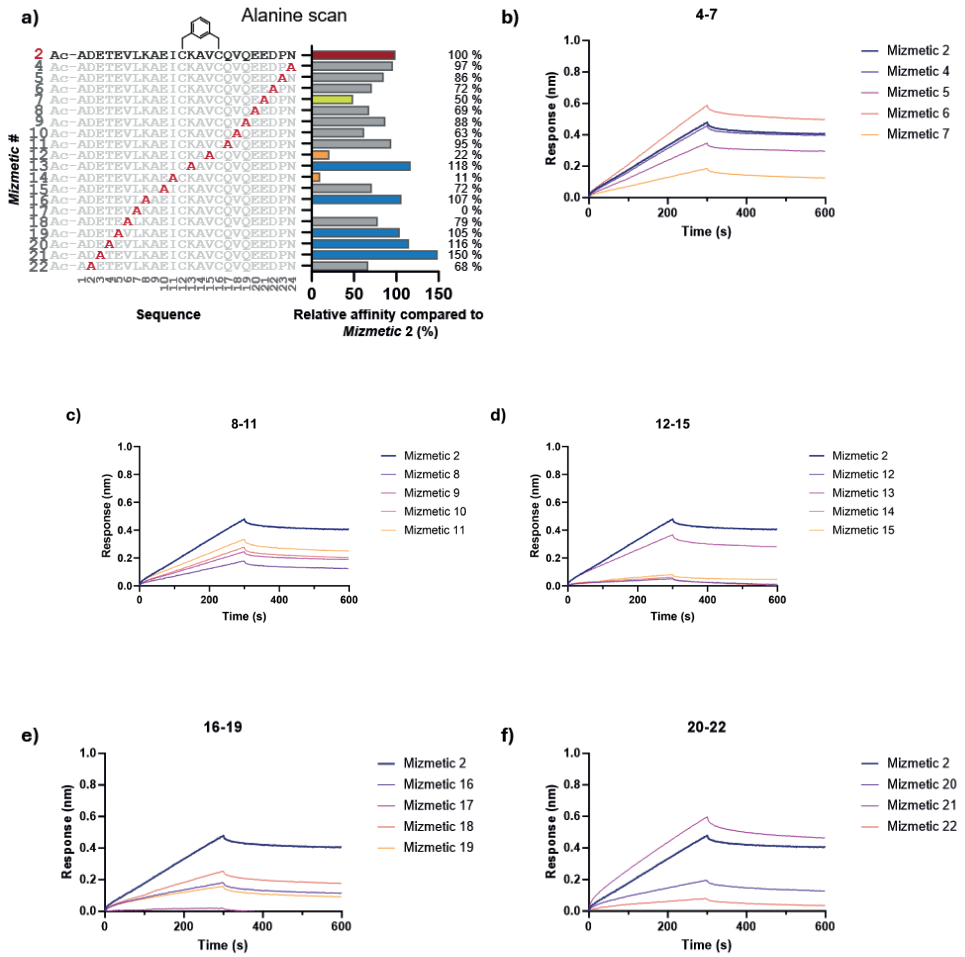

▲Figure S5.9: BLI curves display that Mizmetic 12, 14 and 17 have a decreased affinity towards MYC. Mizmetic 13, 16, 19-21 have increased affinity towards MYC. a) Comparison between affinities of alanine analogues of Mizmetic 2 compared to Mizmetic 2. b) BLI curves belonging to Mizmetic 2 and 4-7. c) BLI curves belonging to Mizmetic 2 and 8-11. d) BLI curves belonging to Mizmetic 2 and 12-15. e) BLI curves belonging to Mizmetic 2 and 16-19. f) BLI curves belonging to Mizmetic 2 and 20-22. All Mizmetics were screened against 400 nM of MYC.

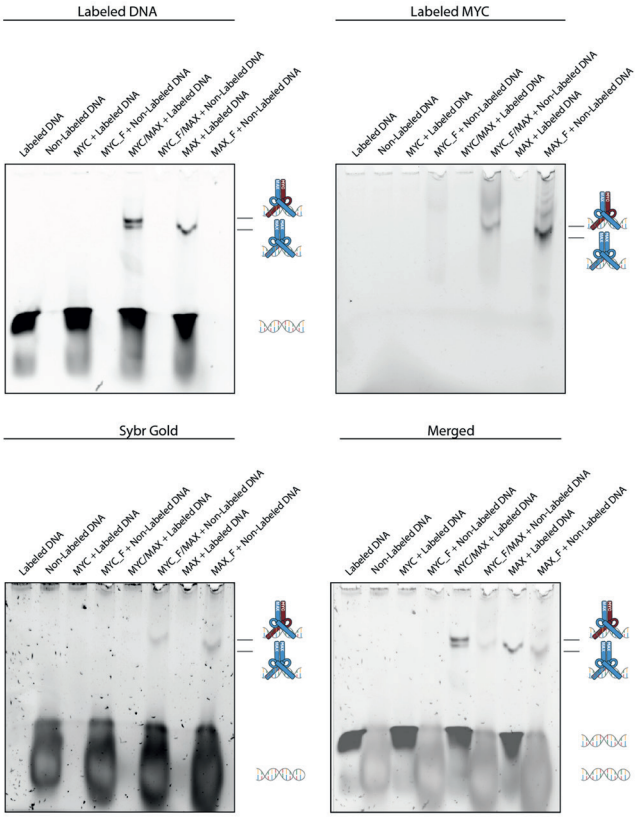

▲**Figure S5.10:** MYC/MAX complex is formed and visible with both labeled MYC_F or with labeled DNA.

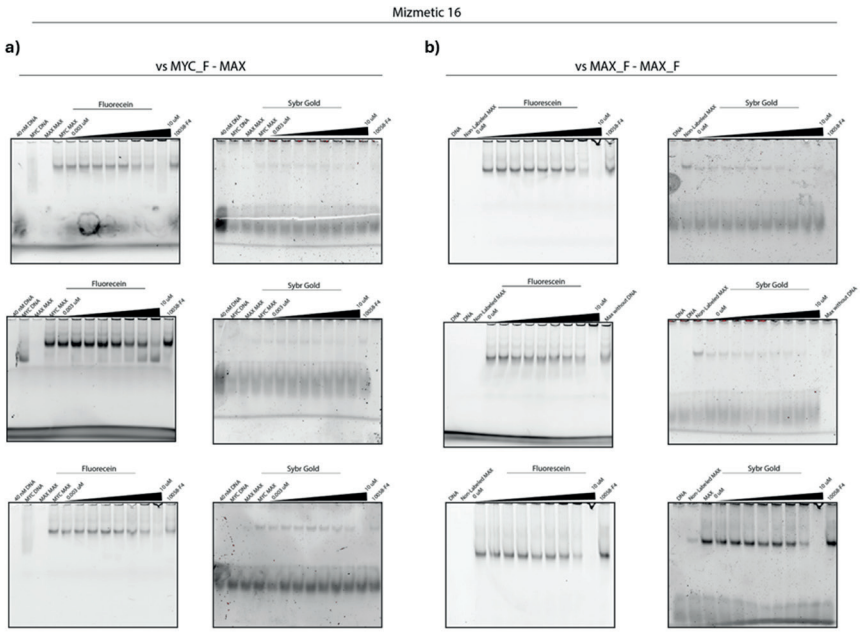

▲**Figure S5.11:** a) Concentration curve against MYC_F and MAX. An IC_{50} of 3.08 µM ± 1.94 µM was observed. b) Concentration curve against MYC_F and MAX. An IC_{50} of 1.94 µM ± 0.71 µM was observed. Mizmetics were stepwise diluted to 4x 10-0.003 µM in DMSO prior to incubation with 4x MYC_F (60 nM) in kinetic buffer. The mixture was incubated at RT for 1h followed by the addition of 4x MAX (60 nM) and 4x DNA (160 nM). The mixtures were incubated for 5 minutes and placed on ice while loading 12.5 µL on gel. Final concentrations Mizmetics (10-0.003 µM), MYC_F and MAX (both 15 nM), DNA (40 nM). Gels ran for 80 min at 75V at 4 °C and were imaged, followed by 15-40 min SYBR gold incubation to visualize DNA.

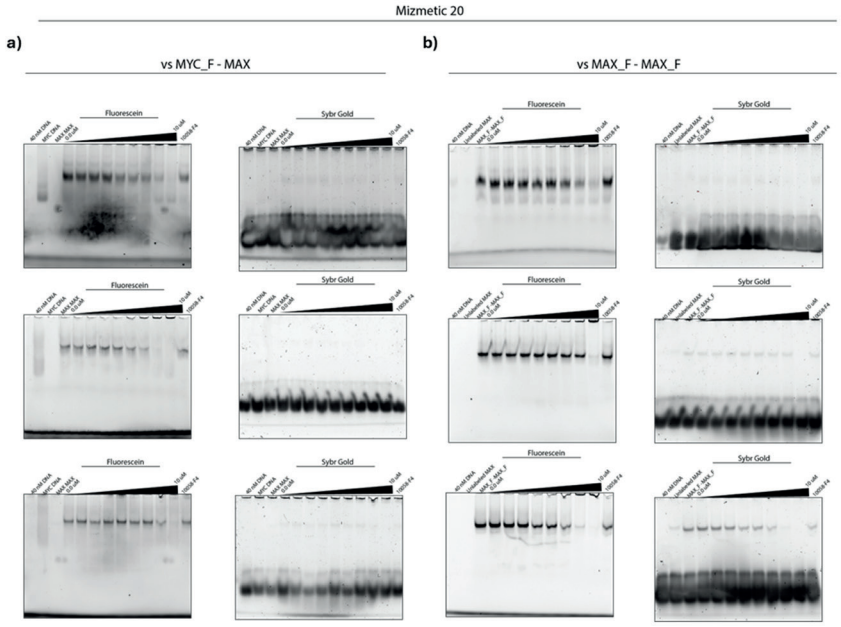

▲**Figure S5.12:** a) Concentration curve against MYC_F and MAX. An IC_{50} of 0.56 µM ± 0.22 µM was observed. b) Concentration curve against MYC_F and MAX. An IC_{50} of 2.25 µM ± 1.93 µM was observed. Mizmetics were stepwise diluted to 4x 10-0.003 µM in DMSO prior to incubation with 4x MYC_F (60 nM). The mixture was incubated at RT for 1h followed by the addition of 4x MAX (60 nM) and 4x DNA (160 nM). The mixtures were incubated for 5 minutes and placed on ice while loading 12.5 µL on gel. Final concentrations Mizmetics (10-0.003 µM), MYC_F and MAX (both 15 nM), DNA (40 nM). Gels ran for 80 min at 75V at 4 °C and were imaged, followed by 15-40 min SYBR gold incubation to visualize DNA.

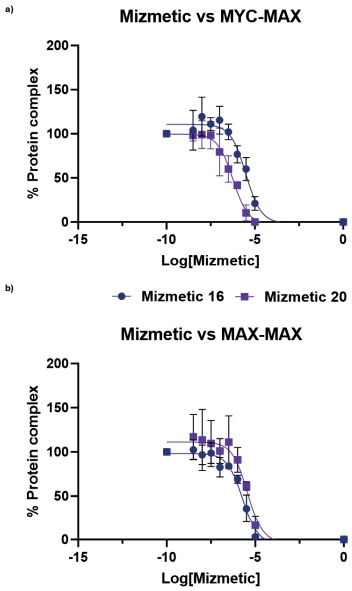

▲Figure S5.13: Mizmetic alanine analogues can inhibit the formation of MYC-MAX or MAX-MAX. a) Quantification of concentration curves of Mizmetic 16 and 21 against MYC_F – MAX. b) Quantification of concentration curves of Mizmetic 16 and 21 against MAX_F – MAX. All experiments were performed at n = 3.

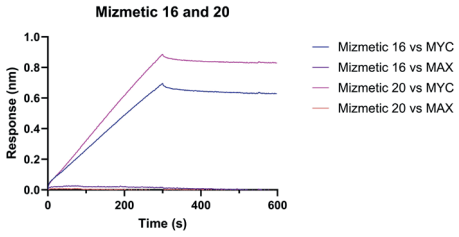

▲Figure S5.14: BLI curves show that Mizmetics have affinity towards MYC but not towards MAX. Mizmetics were screened against 1 μM MYC or MAX.

5.5.7 References

[1] B. D. Ellenbroek, J. P. Kahler, D. Arella, C. Lin, W. Jespers, E. A. Züger, M. Drukker, S. J. Pomplun, ""Development of DuoMYC: a synthetic cell penetrant miniprotein that efficiently inhibits the oncogenic transcription factor MYC,"" *Angewandte Chemie International Edition* **2025**, *64*, , DOI 10.1002/anie.202416082.

[2] A. Micsonai, F. Wien, N. Murvai, M. P. Nyiri, B. Balatoni, Y.-H. Lee, T. Molnár, Y. Goto, F. Jamme, J. Kardos, ""BeStSel: analysis site for protein CD spectra—2025 update,"" *Nucleic Acids Res* **2013**, *1*, 13–14.

[3] A. Micsonai, É. Moussong, F. Wien, E. Boros, H. Vadászi, N. Murvai, Y. H. Lee, T. Molnár, M. Réfrégiers, Y. Goto, Á. Tantos, J. Kardos, ""BeStSel: webserver for secondary structure and fold prediction for protein CD spectroscopy,"" *Nucleic Acids Res* **2022**, *50*, W90–W98.

[4] N. S. A. Crone, A. Kros, A. L. Boyle, ""Modulation of Coiled-Coil Binding Strength and Fusogenicity through Peptide Stapling,"" *Bioconjug Chem* **2020**, *31*, 834–843.

[5] M. J. Huang, Y. chih Cheng, C. R. Liu, S. Lin, H. E. Liu, ""A small-molecule c-Myc inhibitor, 10058-F4, induces cell-cycle arrest, apoptosis, and myeloid differentiation of human acute myeloid leukemia,"" *Exp Hematol* **2006**, *34*, 1480–1489.